1967

Pressure distribution on a fixed surface parallel to a rotating disk

Leo Charles Peters
Iowa State University

PRESSURE DISTRIBUTION ON A FIXED SURFACE PARALLEL TO A ROTATING DISK

by

Leo Charles Peters

A Dissertation Submitted to the

Graduate Faculty in Partial Fulfillment of

The Requirements for the Degee of

DOCTOR OF PHILOSOPHY

Major Subjects: Mechanical Engineering
Engineering Mechanics

Approved:

Signature was redacted for privacy.

In Charge of Major Work

Signature was redacted for privacy.

Heads of Major Departments

Signature was redacted for privacy.

Dean of Graduate College

Iowa State University
Of Science and Technology
Ames, Iowa

1967

TABLE OF CONTENTS

SYMBOLS

C	gap width, inches
F_i	calibration factor for i'th manometer tube, inches of water per inch of reading
F_{ref}	calibration factor for reference manometer tube, inches of water per inch of reading
g	acceleration due to gravity, feet per second squared
K	ratio of angular velocity of fluid to angular velocity of rotating disk (see page 14 and Due [6])
m	mass rate of flow, slugs per second
p	pressure, pounds force per square foot
p_o	pressure at outer radius of disk, pounds force per square foot
p_i	manometer tube reading for the i'th manometer tube, inches
p_{oi}	zero pressure manometer tube reading for the i'th manometer tube, inches (see Figure 7)
p_{ref}	reference manometer tube reading, inches
p_{ref-o}	zero pressure reference manometer tube reading, inches
Q	volumetric throughflow rate, cubic feet per second
r	radius, feet; radial coordinate in cylindrical coordinates
r_o	disk outer radius, feet
R	gas constant, foot pounds-force per pound mass, degree Rankine
s	gap width, feet
T	absolute temperature, degrees Rankine

u	velocity in radial direction, feet per second
u_1	radial velocity with no net throughflow, feet per second
u_2	radial velocity due to net throughflow, feet per second
v	velocity in tangential direction, feet per second
w	velocity in axial direction, feet per second
z	axial distance, feet; coordinate in the axial direction in cylindrical coordinates
z_o	gap width, feet
θ	angular coordinate in a cylindrical coordinate system, radians
γ	specific weight, pounds force per cubic foot
μ	absolute viscosity, pounds force-seconds per square foot
ν	kinematic viscosity, square feet per second
ρ	density, slugs per cubic foot
ω	angular velocity, radians per second

Miscellaneous notation

$\delta( )$	used to indicate the uncertainty of ( )
$\sim$	implies approximately the same order of magnitude

INTRODUCTION

The general problem of a disk rotating in a fluid has been studied for many years in varying configurations. The earliest work on the rotating disk problem concerned rotation of a finite or infinite rigid plane lamina in a Newtonian fluid of infinite extent. The theoretical work during this time centered on determining velocity distributions, pressure distributions and frictional torques; while the experimental work was intended to obtain information to better understand and predict operating characteristics of rotating fluid machinery.

Emphasis then shifted to a consideration of fluid flow resulting from a disk rotating in an enclosed housing, or to flow in a relatively large gap (0.060 inch or larger) between a rotating disk and a stationary plate. The flow characteristics usually determined in these two situations were velocity distributions, mode of flow and power absorption. The pressure distribution was either calculated to complete the description of the flow field or was measured to establish other characteristics of the flow.

Not until recently has interest been manifested in the pressure distribution as a primary flow characteristic and in the characteristics of fluid flow in narrow gaps (less than 0.060 inch) between a rotating disk and a stationary parallel plate. This interest was motivated by the advent of similar

fluid flow applications in gas lubricated bearings, high pressure centrifugal pumps and oil lubricated clutches. The performance in each of these applications is markedly affected by the pressure distribution at the plate surface. Prediction of the pressure distribution in these applications requires a knowledge of the velocity distributions present.

An examination of the literature reveals a general lack of information on fluid flow in narrow gaps between rotating disks and stationary plates. Only three papers were found that specifically covered this flow situation, and all three were limited in scope. One was a theoretical study with much background information omitted. Another was limited to small flows with no explanation of what happened for higher flows. Neither of these papers indicated any direct verification of theoretical results by experimental means. The third report, which was primarily experimental, determined empirical pressure distribution equations based on low flows using water and liquid hydrogen as fluids.

In summary, applications of fluid flow in a narrow gap between a rotating disk and a parallel stationary plate exist today and no organized basic approach has been found for determining either the characteristics of the flow or the parameters affecting them. This investigation was initiated to determine the basic parameters that affect this flow situation and to relate them to appropriate terms in the governing

equations. Verification of the influence of the basic parameters was attempted by experimentally determining pressure distributions for various rates of flow in gaps (0.040 inch or less) between a rotating disk and a parallel stationary plate. The basic system is shown in a sketch in Figure 1.

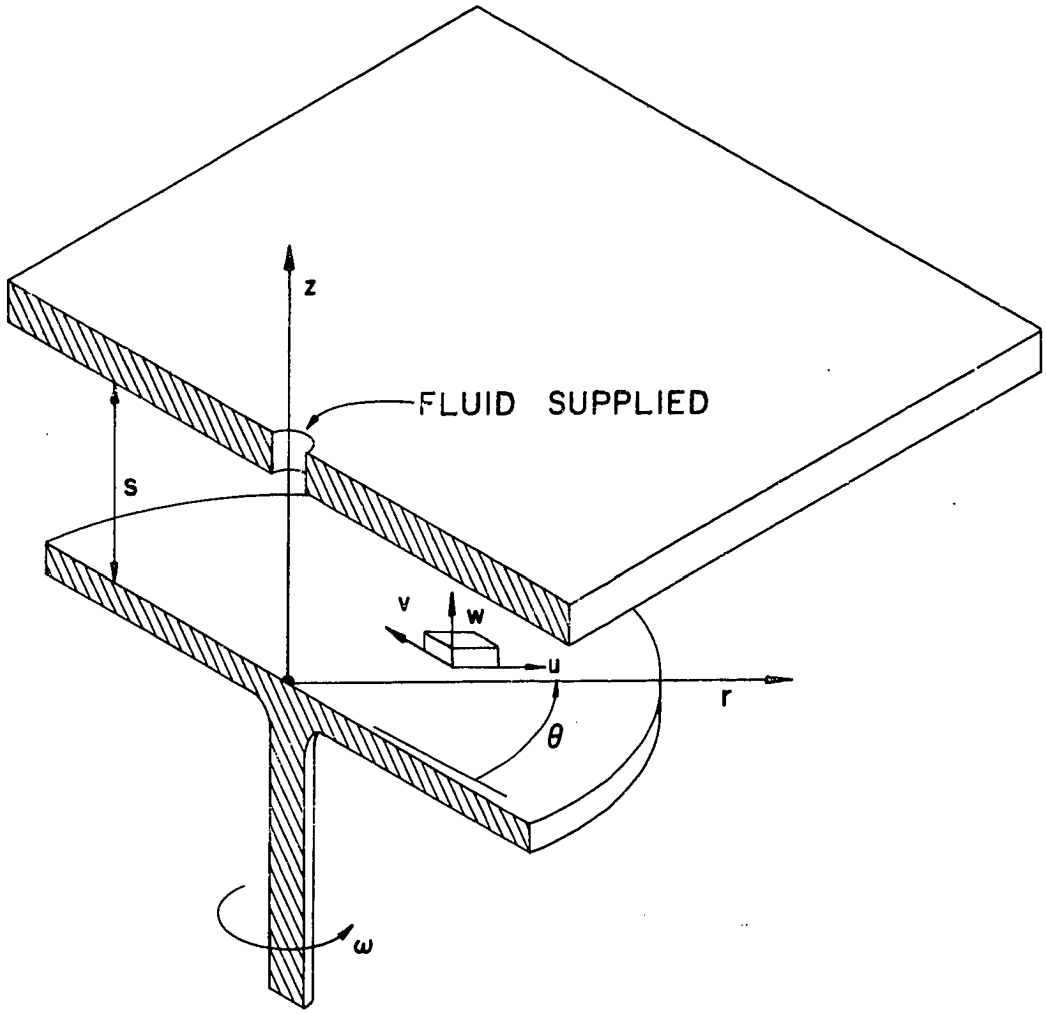

Figure 1. Sketch of basic system

REVIEW OF LITERATURE

Much of the work done previously on rotating disks was performed to determine pertinent variables affecting power loss or the power loss resulting from a disk rotating in the presence of a fluid. An extensive historical review of the literature concerning this work with rotating disks in the presence of a fluid may be found in Peters (14).

Interest in pressure distributions existing in a fluid flowing in a gap between a rotating disk and a stationary parallel plate has only recently been developed. Among the earliest reports concerned with this problem were those made by Reiner (16) and Popper and Reiner (15). A device was constructed consisting of a rotating disk, 2.54 inches in diameter, and a stationary plate which could be brought very close together. The gap width was controllable between 0.75 mm and 0.015 mm (0.0295 to 0.00059 inch respectively). The rotating disk was run at 7000 rpm. When a hole at the center of the stator was connected to a manometer for the 0.75 mm gap, a suction of approximately one centimeter of water was observed. When the gap was reduced to approximately 0.02 millimeter (0.000788 inch), a pressure greater than one-half atmosphere was observed. This behavior was attributed to a non-Newtonian or viscoelastic property of air analogous to that exhibited by some rubber solutions.

Taylor and Saffman (18), after viewing Reiner's test

device and reviewing his conclusions, performed a theoretical analysis which showed that a small angle between disks or axial vibration of the rotating disk could cause the same phenomena to be observed. They then attempted an experimental verification of their theory. They did show that at very small gaps (on the order of 0.00012 inch) a positive pressure, instead of a suction, was obtained at the center of the disk. As the test was being run the rotating shaft expanded longitudinally, closing the gap and destroying the disks before any gap width measurements could be made.

The primary concern in subsequent investigations was with the power required to drive a rotating disk in a fluid. Determination of the power requirements necessitated a knowledge of the flow mode (i.e., laminar or turbulent, steady or unsteady) and the velocity distribution in the fluid. Only a limited amount of pressure distribution data was presented in the following investigations.

Welsh and Hartnett (19) investigated modes of flow for the case of two parallel coaxial disks rotating in air in the same direction at the same angular velocities. The spacing between disks was changed from run to run and ranged from 4 to 8 inches. Only one typical set of curves showing both static and total pressure profiles was presented.

Daily and Nece (5) determined analytically and experimentally the modes of flow, drag coefficient and velocity and

pressure information for a disk rotating in a completely enclosed housing with no throughflow. Gap widths used ranged from 0.125 to 2.13 inches and fluids used were water and oil.

Maroti, Deak and Kreith (11) investigated the flow of air between a rotating disk and a wall of larger diameter. Distinct and separate inflow and outflow regions were observed to rotate in the same direction as the disk but at a lower angular velocity. Gap widths used were 0.125 to 1.0 inch. A source flow superimposed on the fluctuating flow decreased the intensity of the flow reversals and, eventually, produced steady radial outflow as the source flow was increased.

Daily and Arndt (3) and Daily, Ernst and Asbedian (4) investigated the basic effects and the steady and unsteady characteristics of induced flow for enclosed rotating disks with superposed throughflow. Gap ratios ranging from 0.0138 to 0.069 (gap widths ranging from 0.25 to 0.63 inch) and throughflow rates ranging from zero to 26 cubic feet per minute for air and zero to 2.64 cubic feet per minute for water were used in their investigations. Modes of flow were determined using velocity measurements in the gap and flow visualization techniques.

Bayley and Conaway (1) performed an experimental investigation to determine the effect of pertinent variables on the drag torque and the radial pressure distribution on a plate parallel to a rotating disk. Flow was developed by applying a suction to the stationary plate directly across the gap from

the axis of rotation of the disk. This caused the throughflow to be inward from the disk outer diameter. The gap widths used ranged from 0.060 to 0.090 inch, the disk diameter was 30 inches, the Reynolds number (defined as $\frac{\omega r_o^2}{\nu}$) range was from zero to 4×10^6 and the mass flow coefficient (defined as $\frac{\rho Q}{\mu r_o}$ using the notation of this investigation) ranged from zero to 10^4.

The following three studies were the only ones reported in the literature that were conducted using the ranges of variables employed in this investigation.

Two analyses, based on the Navier-Stokes equations, have been performed to determine the velocity distribution and the radial pressure gradient between a rotating disk and a parallel stationary plate for low flows and small gaps.

Soo (17) performed a theoretical analysis of laminar fluid flow over an enclosed rotating disk. He started with the Navier-Stokes equations in cylindrical coordinates and the continuity equation, then assumed steady flow over a disk rotating at constant angular velocity, ω. He introduced boundary layer approximations to reduce the Navier-Stokes equations to the following equations

$$u\frac{\partial u}{\partial r} + w\frac{\partial u}{\partial z} - \frac{v^2}{r} = -\frac{1}{\rho}\frac{\partial p}{\partial r} + \nu\frac{\partial^2 u}{\partial z^2} \qquad (1)$$

$$\frac{u}{r}\frac{\partial (rv)}{\partial r} + w\frac{\partial v}{\partial z} = \nu\frac{\partial^2 v}{\partial z^2} \qquad (2)$$

$$\frac{\partial p}{\partial z} = 0 \quad . \tag{3}$$

The boundary conditions for these equations are

$$u(r,0) = 0 \tag{4}$$

$$u(r,z_o) = 0 \tag{5}$$

$$v(r,0) = r\omega \tag{6}$$

$$v(r,z_o) = 0 \tag{7}$$

$$w(r,0) = 0 \tag{8}$$

$$w(r,z_o) = 0 \tag{9}$$

$$2\pi\rho\int_0^{z_o} rudz = m \tag{10}$$

A stream function, ψ, was defined by

$$w = \frac{1}{r}\frac{\partial(r\psi)}{\partial r} \tag{11}$$

$$u = -\frac{\partial\psi}{\partial z} \quad , \tag{12}$$

and was given explicitly as

$$\psi = \left(\frac{\omega z_o^2}{\nu}\right) r\omega z_o W(\zeta) + \frac{m}{2\pi\rho}U(\zeta) \quad , \tag{13}$$

also

$$v = r\omega V(\zeta) \quad , \tag{14}$$

where $U(\zeta)$, $V(\zeta)$ and $W(\zeta)$ are dimensionless functions of ζ, which are to be determined.

The term ζ is defined as

$$\zeta = \frac{z}{z_o} \quad . \tag{15}$$

Soo (17) eliminated the pressure in Equation 1 by taking $\frac{\partial}{\partial r}$ of Equation 3 and $\frac{\partial}{\partial z}$ of Equation 1, then setting the resulting equations equal to each other. He determined u and w by using Equations 11 and 12 and substituted u, v and w into the equation resulting from $\frac{\partial}{\partial z}$ of Equation 1 and Equation 2. Assuming that the mass rate of flow was small and that the quantity $\left(\frac{\omega z_o^2}{\nu}\right)$ was very small, he developed the following equations

$$u = - \frac{\omega z_o^2}{\nu} r\omega W'(\zeta) - \frac{mU'(\zeta)}{2\pi\rho z_o r} \tag{16}$$

$$v = r\omega V(\zeta) \tag{17}$$

$$w = 2\left(\frac{\omega z_o^2}{\nu}\right)\omega z_o W(\zeta) \tag{18}$$

where

$$V(\zeta) = 1 - \zeta \tag{19}$$

$$W(\zeta) = - \frac{\zeta^2}{20} + \frac{7}{60}\zeta^3 - \frac{\zeta^4}{12} + \frac{\zeta^5}{60} \tag{20}$$

$$U'(\zeta) = 6\zeta - 6\zeta^2 \tag{21}$$

$$W'(\zeta) = -\frac{\zeta}{10} + \frac{7}{20}\zeta^2 - \frac{\zeta^3}{3} + \frac{\zeta^4}{12} \quad . \tag{22}$$

Soo (17) stated that m was to be positive for outward throughflow. According to a sketch in his paper, the positive direction for u is the same as for a positive r (i.e., outward from the center of the disk). Intuitively then, u should be positive for outward throughflow. Inspection of Equation 16 reveals that the first term on the right hand side of the equals sign gives the portion of u attributed to centrifugal force acting on the fluid and the second term provides the portion of u due to the throughflow. Examination of Equation 22 reveals that since $0<\zeta<1$, $W'(\zeta)$ is negative, so the resulting first term in Equation 16 is positive. Inspection of Equation 21 also indicates that for $0<\zeta<1$, $U'(\zeta)$ is positive and if m is positive in Equation 16, then the portion of u due to outward throughflow is negative. This cannot be since the velocity has to be in the direction of the throughflow (i.e., positive).

If ψ is changed by making the second term in Equation 13 negative, then this makes the second term in Equation 16 positive and shows that the portion of u due to the throughflow is in the same direction as the mass flow. The revised stream function still satisfies the continuity equation. The

suggested error in sign of the second term of the stream function does not change Equations 19 through 22.

Soo (17) obtained the equation for pressure distribution by substituting Equations 16 through 22 into Equation 1, then integrating each term from zero to z_o with respect to z and dividing each term by z_o to obtain an average value. The resulting equation for the pressure gradient was integrated from some arbitrary radius to a reference radius and was presented as an equation for the Euler number $\left(\frac{p-p_o}{\frac{1}{2}\rho\omega^2 r_o^2}\right)$.

A check of his development of this equation revealed apparent errors in the derivation, in addition to using a possibly incorrect equation for u. A corrected equation developed using Soo's (17) method is

$$\frac{p-p_o}{\frac{1}{2}\rho\omega^2 r_o^2} = -\frac{12}{\pi\left(\frac{\omega z_o^2}{\nu}\right)}\left[\frac{m}{\rho z_o \omega r_o^2}\right]\ell n\frac{r}{r_o} - \frac{3}{10\pi^2}\left[\frac{m}{\rho z_o \omega r_o^2}\right]^2\left[\frac{r_o^2}{r^2}-1\right]$$

$$+\frac{3}{10}\left[\frac{r^2}{r_o^2}-1\right] \qquad (23)$$

No experimental data accompanied Soo's (17) presentation of theoretical velocity distributions or theoretical pressure distribution.

Pelech (12) and Pelech and Shapiro (13) present a theoretical solution for the problem of fluid flow resulting from the

rotation of a flexible disk close to a wall. This problem resulted from the development of a flexible disk magnetic memory for a small digital computer. The fluid flow was self-induced from the axis of rotation of the disk to the outer diameter of the disk. Gap widths were on the order of 0.001 inch. As a portion of the solution of this problem, Pelech and Shapiro (13) simplified the Navier-Stokes equations using order of magnitude methods, then solved for a constant gap width. The important dimensionless terms were shown to be

$$\frac{s}{r_o} \tag{24}$$

$$\left(\frac{\omega r_o^2}{\nu}\right)^2 \left(\frac{s}{r_o}\right)^4 \tag{25}$$

$$\frac{Q}{r_o^2 \omega s} \quad . \tag{26}$$

These dimensionless terms were related to the ratio of the magnitude of the convective terms to the $\frac{v^2}{r}$ term in Equation 1. It was shown that for their problem, the magnitudes of the above terms were much less than 1, thus allowing all convective terms to be neglected. As a result the Navier-Stokes equations were linearized, allowing expressions to be found for u, v and w. These equations were then substituted into Equation 1 without the first two terms and the following expression for pressure gradient in the r direction was developed

$$\frac{dp}{dr} = \frac{3}{10}\rho\omega^2 r - \frac{6\mu Q}{\pi r s^3} \quad . \tag{27}$$

No attempt was made in their work to experimentally verify this equation.

Due (6), using experimental data, determined semi-empirical equations for the radial pressure distribution occurring in a fluid flowing with a small net throughflow in the gap between either a smooth or a bladed disk and a stationary plate. Only the equations developed from the smooth disk data are considered in this investigation. One equation was developed using water as a fluid; the other using liquid hydrogen. According to his paper, this work was motivated by the inadequacy of currently available methods for predicting thrust-loading on rotors of high-speed centrifugal pumps.

Due's (6) equations were developed as follows. The centrifugal force acting on a rotating ring of fluid was equated to the radial pressure difference required to maintain equilibrium. Viscosity effects were neglected. The resulting expression was integrated between two arbitrary radii (R_1 and R_2), and the angular velocity of the fluid ring was assumed to be a fraction, K, of the disk angular velocity. The following equation was then presented

$$p_2 - p_1 = \frac{\gamma}{2g} K^2 \omega^2 (R_2^2 - R_1^2) \quad . \tag{28}$$

This equation was used to calculate K for test runs with both fluids.

The fraction, K, was then assumed to be a function of certain significant test variables and was correlated with these variables using a statistical regression analysis. The following equations were determined from the regression analysis.

For liquid hydrogen,

$$K = 0.906 + 0.012\phi\left(\frac{C}{R_o}\right)^{-1.0} - 5.36\phi - 51.1\left(\frac{C}{R_o}\right) + 1295.3\left(\frac{C}{R_o}\right)^{2.0} . \quad (29)$$

For water,

$$K = 0.578 - 4.11\phi - 1.67C . \quad (30)$$

In Equations 29 and 30, $\frac{C}{R_o}$ is the gap ratio and is dimensionless; ϕ is the ratio of the throughflow fluid velocity at the disk outer radius to the tangential disk velocity, also at the outer radius. The gap width in Equation 30 (C) is in inches.

The equations for K, developed from the water test data, were considered to be applicable to incompressible fluids at Reynolds numbers greater than 10^6 and in the ranges of the variables used in the tests. Because of the large variations in density and specific heat due to temperature changes, the

equations developed from the liquid hydrogen data were recommended for use only with liquid hydrogen.

A summary of the Review of Literature is presented in Table 1. In the interest of completeness, some data are found in Table 1 that were not included in the preceding discussion.

Examination of Table 1 reveals a lack of work done involving narrow gaps between a rotating disk and a stationary parallel plate. Those investigations listed as having used narrow gaps (Reiner, 16; Taylor and Saffman, 18; Pelech and Shapiro, 13) provided only general information and some theory without experimental verification. Thus, it appears that there is a need for investigations in this area to provide information that could be used in the applications discussed in the introduction as well as to lead to a better understanding of the nature of the fluid flow in this situation.

Table 1. Summary of investigations reported in the literature

Investigator	Disk diameter (inches)	Gap width (inches)	Through-flow rates	Disk Reynolds No. range or RPM when noted	Fluid	Comments
Reiner (16) and Reiner & Popper (15)	2.54	0.0295 to 0.00059	not given	7000 rpm	air	Exhibition device only
Taylor & Saffman (18)	4	0.00059	not given	2500 rpm	air	Mostly theoretical work; experiment failed
Welsh & Hartnett (19)	18	4 to 8	not measured	2.35 to 6.19×10^5	air	Both disks rotated in the same direction at the same speed
Daily & Nece (5)	19-5/8	0.125 to 2.13	zero	10^3 to 10^7	water & oil	Disk in a completely enclosed housing with no throughflow
Maroti, Deak & Kreith (11)	20 & 16	0.125 to 1.000	zero, not measured	3×10^5 to 6×10^6	air	Disk between two side walls of larger diameter. No through-flow data provided
Daily et al. (3,4)	18-1/8	0.25 to 0.63	zero to 26 CFM	2.9×10^5 to 8.5×10^6	air & water	Same fixture as Daily & Nece (5)

Table 1. (continued)

Investigator	Disk diameter (inches)	Gap width (inches)	Through-flow rates	Disk Reynolds No. range or RPM when noted	Fluid	Comments
Bayley & Conaway (1)	30	0.060 to 0.090	zero to 260 CFM	zero to 10^4	air	Flow was from disk outer diameter to disk center
Soo (17)	--	--	--	--	--	Theoretical analysis only
Pelech & Shapiro (12,13)	3.75 5.00 6.13	Variable 0.002 to 0.013	zero to 0.00418 CFM	1800 rpm 3600 rpm	air	Flexible disk, gap width varied, flow was self induced
Due (6)	11	0.024 to 0.138	not given	6.87 to 22.5×10^6 77.2 to 123×10^6	water liquid hydrogen	Used data to develop semi-empirical equations for pressure distribution

TEST PROGRAM

Equipment

An overall view of the test equipment is shown in Figure 2. Figure 3 is a schematic drawing of the rotating disk, the glass plate and the instrumentation. A top view of the glass plate and rotating disk area is shown in Figure 4. Figure 5 is a detail drawing of the glass plate showing hole locations and general configuration. Figure 6 schematically shows the pressure tap adapter and insert configuration along with the gap measuring instrumentation.

The test equipment was selected and designed so that future investigations involving flow visualization, fluids other than air and unsteady disk rotation could be pursued.

The rotating disk was driven through a flexible coupling by a D.C. motor. A D.C. motor was chosen because of the ease in changing speed. The disk speed was adjusted by changing a setting on a rheostat in the motor field. The disk rotated in a clockwise direction (viewed from the top), and was mounted horizontally to eliminate any varying fluid force components due to gravity.

A torquemeter and slip-ring assembly were mounted on the disk drive shaft, but were not used in this investigation since the torques developed were less than the sensitivity of the torquemeter.

The rotating disk and plate assembly were located

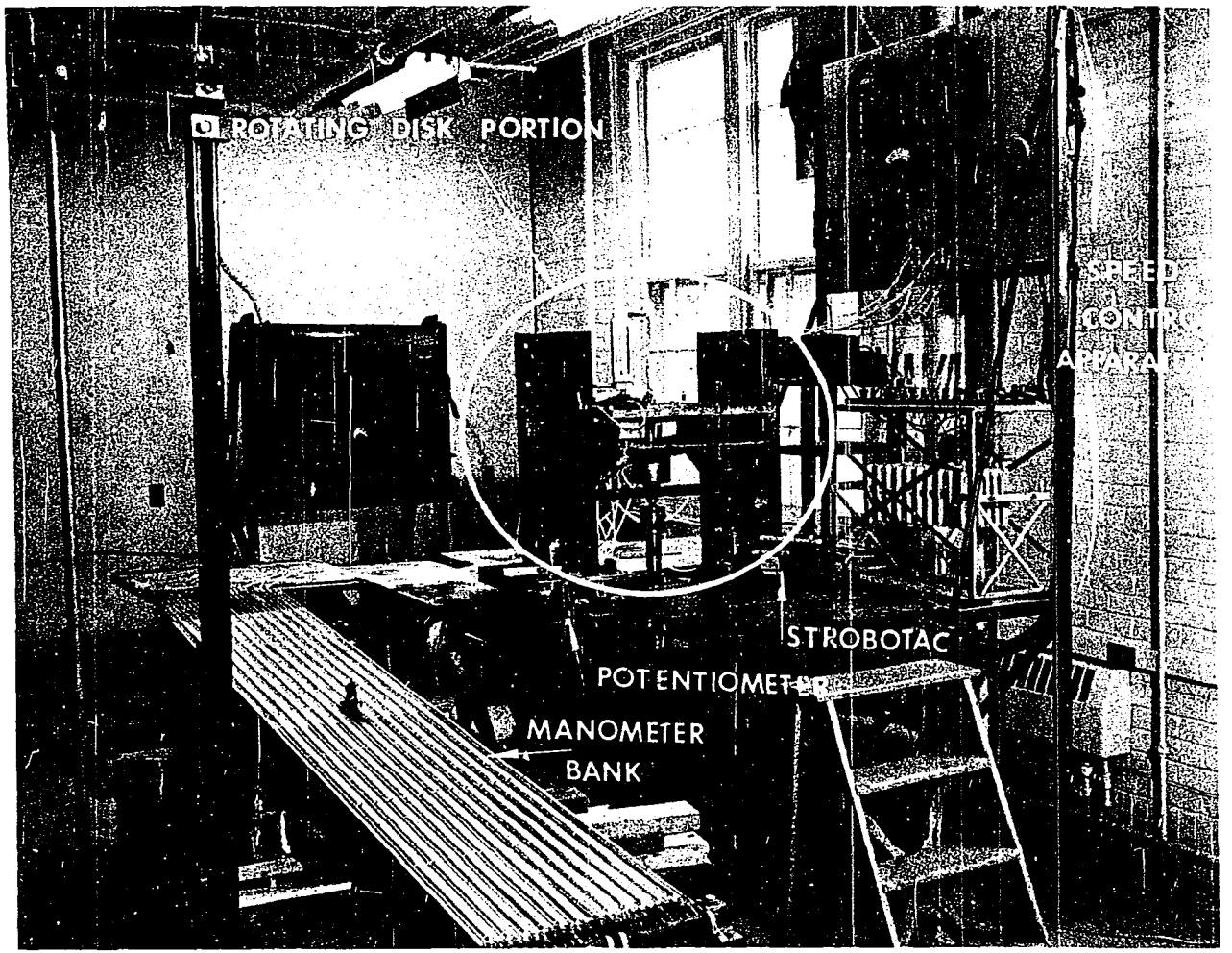

Figure 2. Overall view of experimental equipment

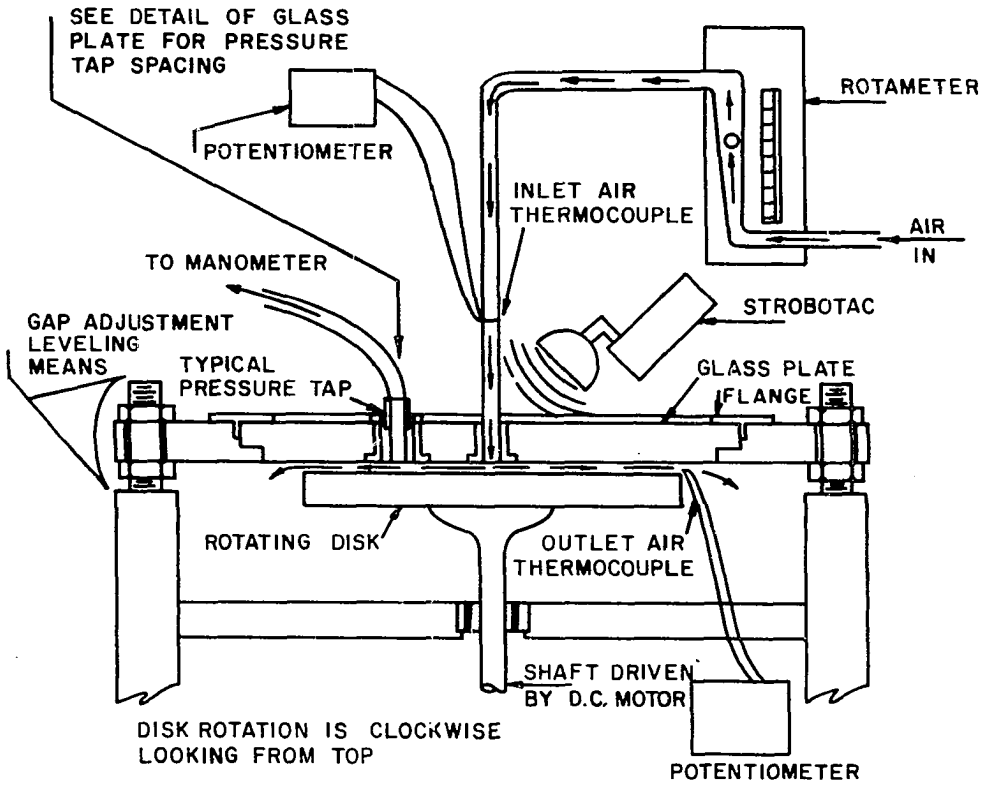

Figure 3. Schematic drawing of rotating disk, stationary plate and instrumentation

approximately six feet above the floor. This was necessitated, in part, because of the length of the motor and drive shaft and in part to provide ready accessibility for assembly and maintenance of the torque meter and slip-ring assembly and any other instrumentation required on the drive shaft in future test work. Portions of the platform may also be removed to gain access to the motor or the instrumentation.

The fixed plate consisted of a steel plate, one inch thick, having a glass plate (shown in Figure 4) mounted in its center in a bed of silicon rubber. The glass plate was included to permit flow visualization studies to be made in the future. Figure 3 shows the composite fixed plate in cross-section. Figure 5 shows the hole pattern and a cross-section of a typical hole. The inserts shown in Figure 6 were selectively machined to fit the holes and were installed in a bed of silicon rubber. The inner diameter of each of the inserts was tapped for 9/16-18NF-2B thread so that adapters could be installed as required. For this set of tests, adapters with a 0.25 hole through were provided. The upper end of each adapter was provided with 1/8-inch pipe threads.

Problems were encountered in mounting the inserts flush with the flat surface of the glass plate due to the difficulty of precisely positioning the inserts in the hole and providing a bed of silicon rubber for mounting. Discrepancies from flush mounting are shown in Table 2 along with the measured

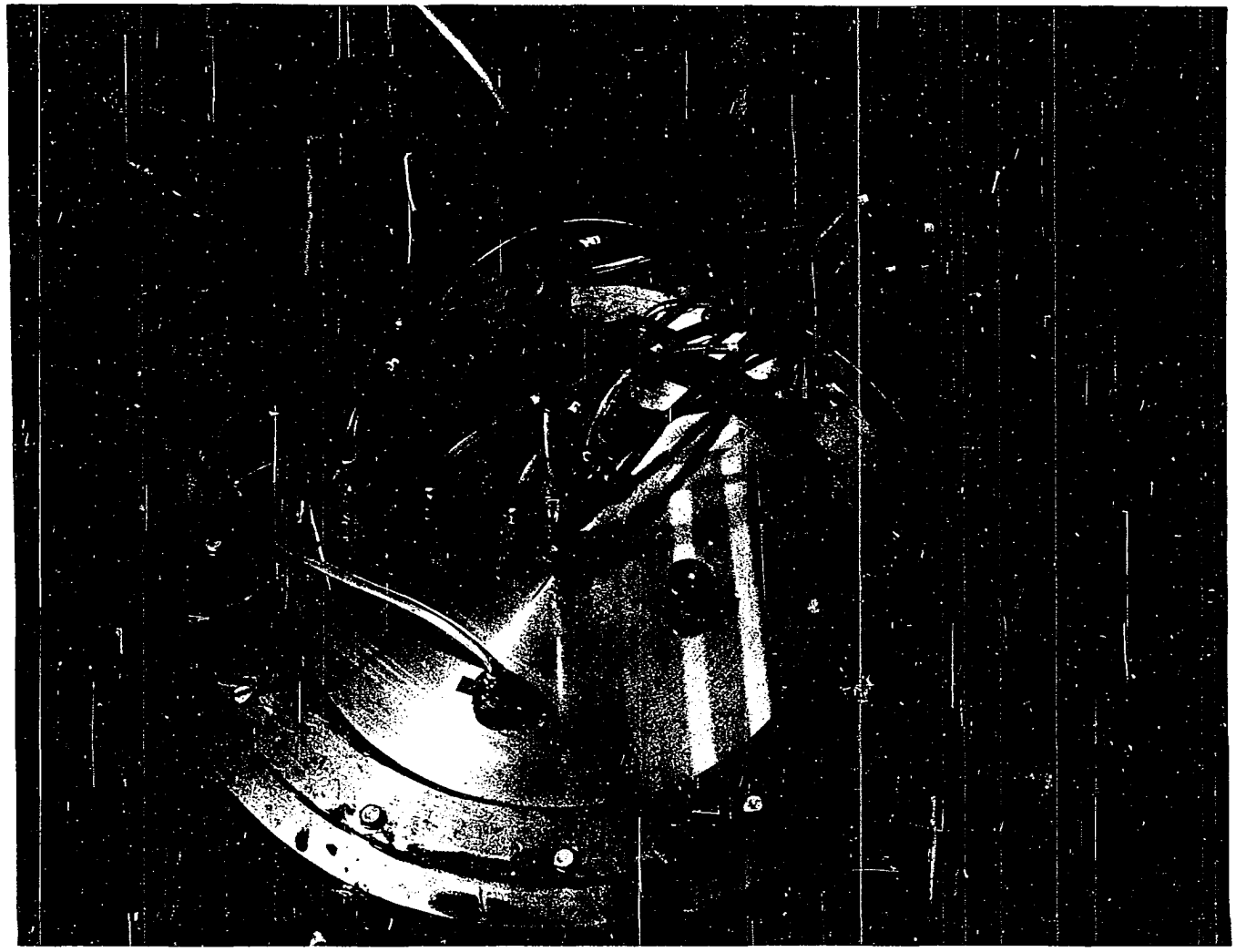

Figure 4. Rotating disk as seen through stationary glass plate

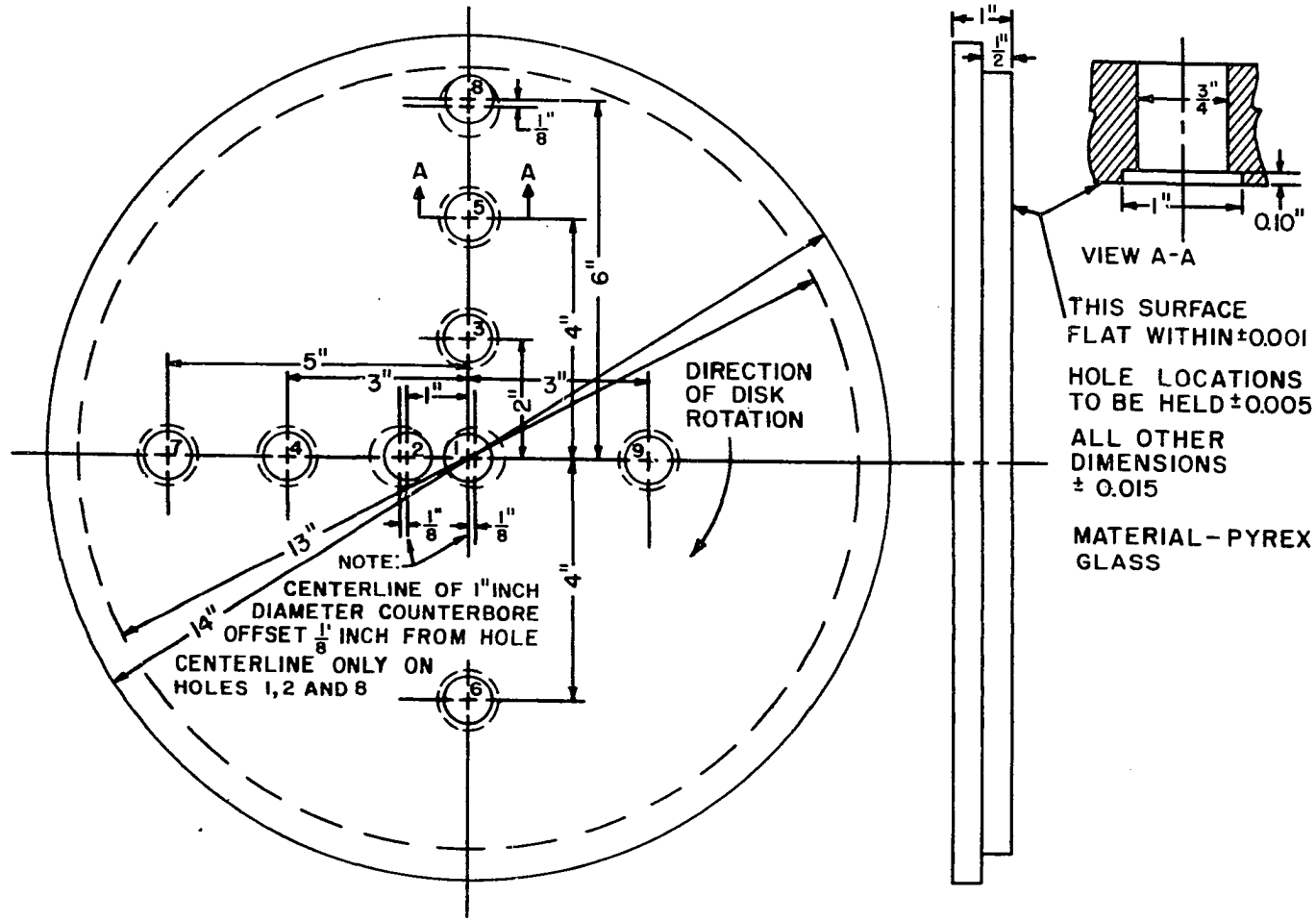

Figure 5. Detail drawing of glass plate

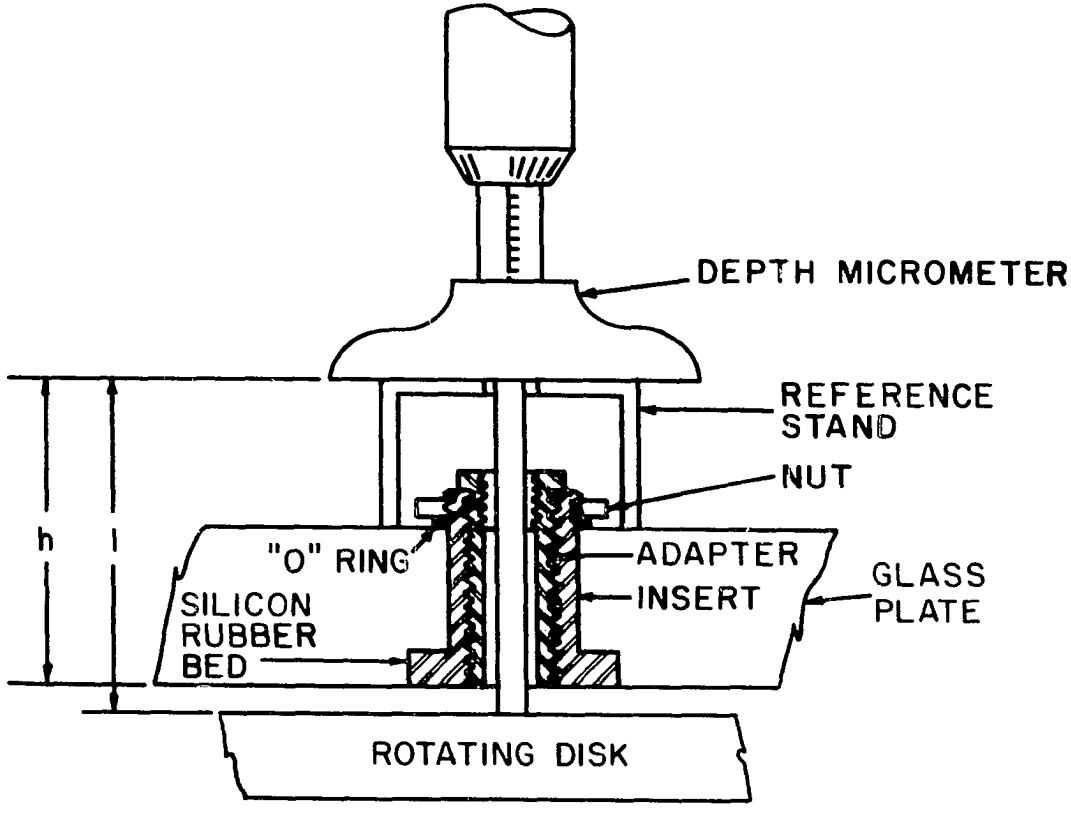

Figure 6. Schematic drawing of pressure tap insert configuration and equipment for measuring gap width

Table 2. Pressure tap insert measurements

Hole No.	Measured radius to hole centerline (inches)	Elevation with respect to surface glass (inches)
1	0.000	-.004[a]
2	1.004	-.002
3	2.022	-.006
4	3.016	-.002
5	4.020	+.003
6	4.024	-.001
7	5.021	-.0015
8	6.020	-.008
9	3.006	-.002

[a]A negative sign in Table 2 implies a recessed insert, a positive sign implies a projecting insert.

radius from the center hole centerline to the centerline of each hole.

Before the initial data runs, an attempt was made to fill the recessed inserts with plaster of Paris, but a satisfactory bond could not be established between the plaster of Paris and the metal and glass. No effort was made to grind the projecting insert down before the initial data runs because of the possibility of breaking or cracking the glass plate. Since the air inlet insert (Hole No. 1) was recessed approximately 0.004 inches, a manifolding effect was present at the air inlet, and the effective air inlet diameter was greater than the 0.25 hole through the adapter. The test runs made under

these conditions are indicated in Figures 8 through 13 as having an inlet diameter of one inch.

Following the initial data runs the projecting insert and adapter combination were ground flush and the recessed insert and adapter combinations were filled with automotive glazing compound. Measurements showed that all adapter and insert combinations were mounted flush to 0.0015 maximum recess. Runs made after these changes are indicated in Figures 8 through 13 as having an inlet diameter of 0.25 inch because the inlet cavity 0.004 inch deep and 1 inch in diameter was filled.

The effects of the grinding and filling operation are discussed in the Results section.

Test Procedure

The controlled variables for each test run were the angular velocity of the disk, the volumetric rate of air throughflow and the width of the gap between the rotating disk and the stationary plate. The measured variable was a pressure reading at each of seven radii. Table 3 gives the values of the controlled variables used in the test runs.

The range of values of gap width chosen are typical of clearances found in disengaged wet clutches and are within reason for clearance values in rotating fluid machinery. In addition, no report of any test work using these values of

Table 3. Values of controlled variables

Angular velocity (rpm)	Flow rate (cubic feet per minute)	Average gap width (nominal, in inches)
2000	0.216	0.040
1800	0.132	0.030
1600	0.084	0.020
1400	0.049	0.010
1200	0.019	0.005
	0.000	

clearance was found in the literature. The flow rate range provides reasonable increments of flow rate, starting with zero, to check the assumption of low flow in Pelech and Shapiro's (13) and Soo's (17) work. The maximum throughflow velocity was approximately 57.5 feet per second. The angular velocity range was determined by the capability of the D.C. motor used to drive the shaft.

Radial pressure profiles were determined for all combinations of the variables listed in Table 3 using the 1-inch diameter air inlet. After the insert and adapter combinations were modified, runs were made for all combinations of 0.020 and 0.010 inch gaps, all flows in Table 3 and angular velocities of 2000 and 1200 rpm.

The following order was used for establishing values of the controlled variables for a given run. The gap width was the most difficult to establish, so it was set first. The

angular velocity was set at the desired value by using a rheostat in the D.C. motor field circuit. The air flow was controlled by a valve on the University air supply line and could be adjusted very rapidly, thus was established last for a given run. Manometer readings were then taken after the pressure levels were established.

The gap width was set by varying the height of the nuts that supported the stationary plate (see Figure 3). Before mounting the stationary plate on the test fixture, the distance h (Figure 6) was measured. This was done by rigidly holding a flat piece of masonite against the bottom of the insert, then measuring from the top surface of the reference stand to the masonite using a depth micrometer. This was done for holes 4, 5, 6 and 9 (see Figure 5 for the location of these holes) only once before any test runs were made. Following this initial calibration, the stationary plate was mounted on the fixture with each corner supported by a nut on a stud as shown in Figure 3. By differentially adjusting the nuts on the four studs, the stationary plate attitude and the gap width could be adjusted as desired. Lock nuts both under the support nut and on top of the plate lock the plate in any position required. To measure the gap width, the depth micrometer was set on the reference stand and distance ℓ was measured at holes 4, 5, 6 and 9. The gap width at each hole was then the difference between ℓ and h. The disk was then

turned 90° and the gap width determined again at the same holes. If none of the gap readings differed more than 0.0015 inch from the mean of the reading, the variation was due to disk wobble, and the gap width used in the calculations was the average of the eight readings. If some readings differed more than 0.0015 inch, the gap was adjusted by using the stationary plate levelling screws and the measurement procedure was repeated.

After the gap was set and before the disk started rotating and the air flow was started, zero pressure readings were observed on the manometer tubes. The manometer tubes were connected to holes 1, 2, 3, 4, 5, 6, 7, and 8, all referenced to atmospheric pressure.

Inlet pressure readings were taken in the line leading to hole 1, but are not included in the data presented since they would add nothing significant to this investigation. Hole 9 was used only for gap setting, although an attempt was made to measure static pressure fluctuations using a Kistler piezoelectric pressure transducer and a charge amplifier. The attempt was unsuccessful due to either the absence of fluctuations of pressure, or the relatively low sensitivity of the transducer. No meaningful transducer output was obtained.

For the first run the disk was rotated at 1200 rpm. The inlet air tube was clamped shut to obtain zero flow. After the manometer readings stabilized, they were recorded. The

clamp was removed from the inlet flow tube, the flow was set at the next lowest level and manometer readings were recorded again. This was repeated for each of the flow values listed in Table 3. The flow values were set by opening the air valve until the ball float in the Rotameter was at the correct elevation, thus indicating the correct flow.

After manometer readings were obtained for all flows at a specified angular velocity, the angular velocity was increased to the next highest value and the procedure repeated. After manometer readings had been obtained for all combinations of angular velocity and flow for a given gap setting, the disk was stopped and the air flow was shut off. The manometers were allowed to stabilize and zero pressure manometer readings were recorded again. The average of the two zero pressure manometer readings for each tube was used as the zero pressure reading (p_{oi}) in the calculations.

Only one run was made for each setting, but the readings for the run were checked at least once.

Data Analysis

The following items were recorded for each run:

1. The temperature of the air supplied to the center of the rotating disk
2. The temperature of the air at the disk outer diameter
3. Atmospheric pressure

4. Zero pressure readings for each manometer tube
5. Pressure reading during the run for each manometer tube
6. Rotameter reading (volumetric rate of air flow)
7. Angular velocity of disk
8. Average gap width

The temperatures and the atmospheric pressure were used to calculate the air density and viscosity. Although the temperature range was 82 ± 5°F (including both the variation and uncertainty of the temperature readings) and the atmospheric pressure range was 14.31 ± 0.18 psia during all runs, calculations in the Appendix indicate that the density may be taken to be constant as 0.0714 $\frac{lb_m}{ft^3}$ ± 1.2% and the viscosity may also be taken as constant at 3.86×10^{-7} $\frac{lb_f\text{-sec}}{ft^2}$ ± 0.7%.

Items 4 and 5, above, were used to determine the pressure difference between each pressure tap and the reference pressure (atmospheric pressure).

Figure 7 shows the effect of a pressure greater than atmospheric on the manometer system. The zero pressure readings are labelled $p_{ref\text{-}o}$ and p_{oi}, respectively, for the tube open to the atmosphere and the manometer tube having a positive pressure applied to it. The positive pressure forces the fluid level down in the pressurized manometer tube and raises the fluid level in the reservoir and in the manometer tube that is open to the atmosphere. If p_i is the reading on the

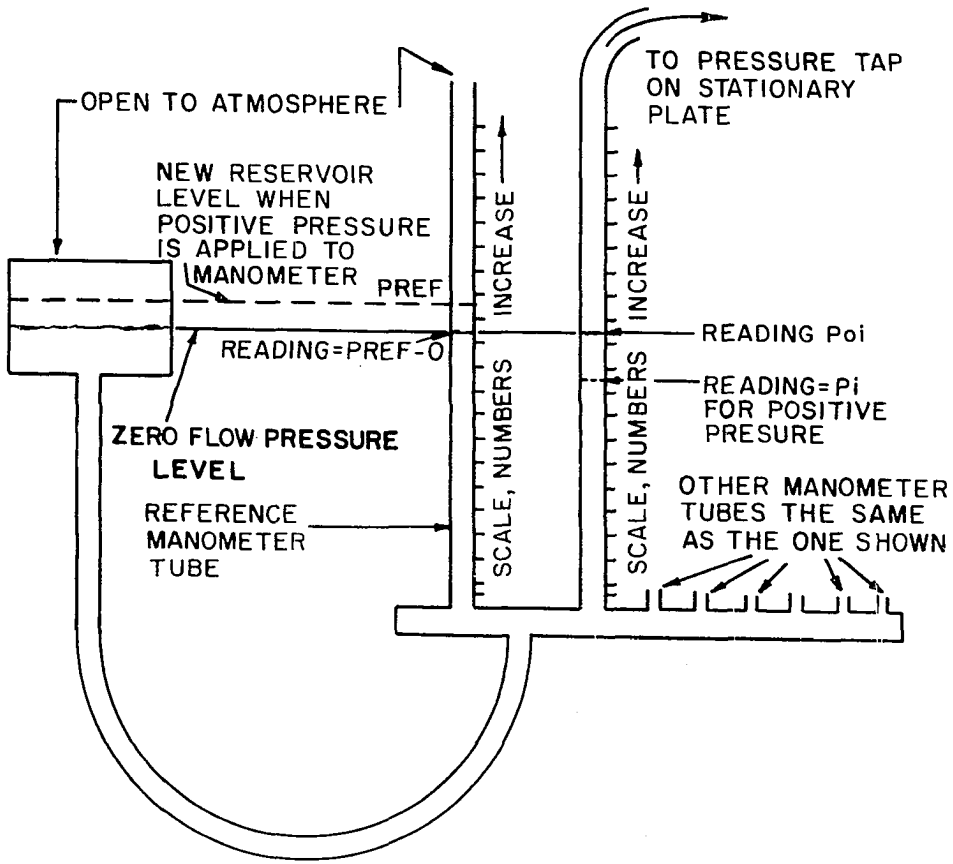

Figure 7. Schematic drawing of manometer bank

pressurized manometer tube and p_{ref} is the reading on the tube open to the atmosphere, then a positive value of $p-p_o$ results from the following equation

$$p-p_o = \left[\frac{p_{oi}-p_i}{F_i} + \frac{p_{ref}-p_{ref-o}}{F_{ref}}\right] 5.204 \frac{lb_f}{ft^2} \quad . \qquad (31)$$

A pressure less than atmospheric will provide a negative value of $p-p_o$ from Equation 31.

The factors F_i and F_{ref} are calibration factors which relate difference in manometer tube readings to pressure difference in inches of water. The manometer bank was designed to be used as a vertical bank, but was inclined for pressure measurements for this test so that a pressure difference of one inch of water would be represented nominally by a ten-inch difference in manometer readings. Each manometer tube used was calibrated individually over its range of operation. The calibration factors and their uncertainties were included in calculating the uncertainty of the pressure difference as indicated in Equation A-10 in the Appendix. Although the uncertainty in pounds force per square foot was on the order of 0.05, the percent uncertainty was comparatively large since the value of the pressure difference could be small. Approximately 95 percent of the values of the percent uncertainty of the pressure drop were between 12 percent and 20 percent.

The volumetric rate of air flow was calculated from calibrated settings on a Brooks Rotameter. The equations used and the uncertainty associated with each setting are discussed in the Appendix. Table 4 lists the flow rates and accompanying uncertainties.

Table 4. Flow and angular velocity values used with associated uncertainties

Flow (CFM)	Flow uncertainty (%)	Angular velocity (radians/second)	Angular velocity uncertainty (%)
0.019	±2.74	209.5	±1.50
0.044	±2.07	188.5	±1.55
0.083	±1.40	167.5	±1.62
0.131	±1.42	146.0	±1.71
0.216	±2.52	125.5	±1.83

The measurement of the angular velocities and the calculation of the associated uncertainties are discussed in the Appendix. The angular velocities and associated uncertainties are tabulated in Table 4.

Calculations for determining the uncertainty of the gap width are shown in the Appendix. The uncertainty for any gap width is 0.00018 inches and the maximum uncertainty in percent is ±3.6 percent for the 0.005 inch gap width. No systematic errors were included in this uncertainty calculation.

A program was written in Fortran IV, for use on the

I.S.U. Computation Center IBM System 360 Model 50 digital computer, to reduce the raw data to dimensionless parameters. Values of the following dimensionless parameters were calculated for all runs

$$\text{Euler number} = \frac{p-p_o}{\frac{1}{2}\rho\omega^2 r_o^2} \tag{32}$$

$$\text{Reynolds number} = \frac{\rho\omega r_o^2}{\mu} \tag{33}$$

$$\text{gap Reynolds number} = \frac{\rho\omega s^2}{\mu} \tag{34}$$

$$\text{flow number} = \frac{\rho Q}{\mu r_o} = N_F \tag{35}$$

$$\text{gap ratio} = \frac{s}{r_o} \tag{36}$$

$$\text{radius ratio} = \frac{r}{r_o} \tag{37}$$

The computer was also used to calculate the uncertainty of the Euler number. Calculations in the Appendix show that the uncertainty of any Euler number is approximately the same as the uncertainty of the pressure drop; thus would lie between

12 and 20 percent for 95 percent of the Euler numbers.

The Reynolds number, flow number and gap ratio may replace angular velocity, volumetric rate of flow and gap width as variables that were changed for this system, thus generalizing the results so they may be compared to similar systems. Tables 5, 6 and 7 list the values of the variables used during the investigation and the value of the corresponding dimensionless parameter.

Pressure taps were located at radius ratios 0.167, 0.357, 0.502, 0.670, 0.836 and 1.000. Euler numbers were calculated for each radius ratio on each run from experimental data.

Table 5. Values of the angular velocity and corresponding Reynolds numbers

Angular velocity (radians/second)	Reynolds number (dimensionless)
209.5	3.01×10^5
188.5	2.70×10^5
167.5	2.40×10^5
146.0	2.10×10^5
125.5	1.80×10^5

Table 6. Values of volumetric rate of flow and corresponding flow numbers

Rate of flow (cubic feet per minute)	Flow number (dimensionless)
0.216	41.35
0.131	25.27
0.083	16.08
0.044	8.42
0.019	3.64
0.000	0.00

Table 7. Values of gap width and corresponding gap ratios

Gap width (inches)	Gap ratio (dimensionless)
0.0400	0.006733
0.0300	0.004916
0.0200	0.003333
0.0106	0.001767
0.0095	0.001583
0.0057	0.000958

RESULTS

Data Presentation

The experimental data are presented as points plotted in Figures 8 through 13. Comparative data are presented as curves in the same figures. Comparative data were calculated from equations derived from Soo's (17) work, Pelech and Shapiro's (13) work and Due's (6) work.

The equation originally presented by Soo (17) for the radial pressure distribution appeared to be in error as discussed in the Review of Literature section. A corrected equation was developed and is

$$\frac{p-p_o}{\frac{1}{2}\rho\omega^2 r_o^2} = -\frac{3}{10\pi^2}\left[\frac{Q}{s\omega r_o^2}\right]^2\left[\frac{r_o^2}{r^2}-1\right]+\frac{3}{10}\left[\frac{r^2}{r_o^2}-1\right]$$

$$-\frac{12}{\pi}\left[\frac{Q}{s\omega r_o^2}\right]\left[\frac{\nu}{\omega s^2}\right]\ln\frac{r}{r_o} \quad . \tag{38}$$

Pelech and Shapiro (13) presented the following equation for the radial pressure gradient

$$\frac{dp}{dr} = \frac{3}{10}\rho\omega^2 r - \frac{6\mu Q}{\pi r s^3} \quad . \tag{39}$$

If Equation 39 is integrated from r_o to any r (r>o) and rearranged, the following equation results

Figure 8. Plot of Euler number versus radius ratio for gap ratio of 0.006733, comparing experimental values determined using air as a fluid with empirically determined values using water as a fluid (Due, 6) and values calculated from theoretical equations (Pelech and Shapiro, 13; Soo, 17) ($N_F = Q/\nu r_o$)

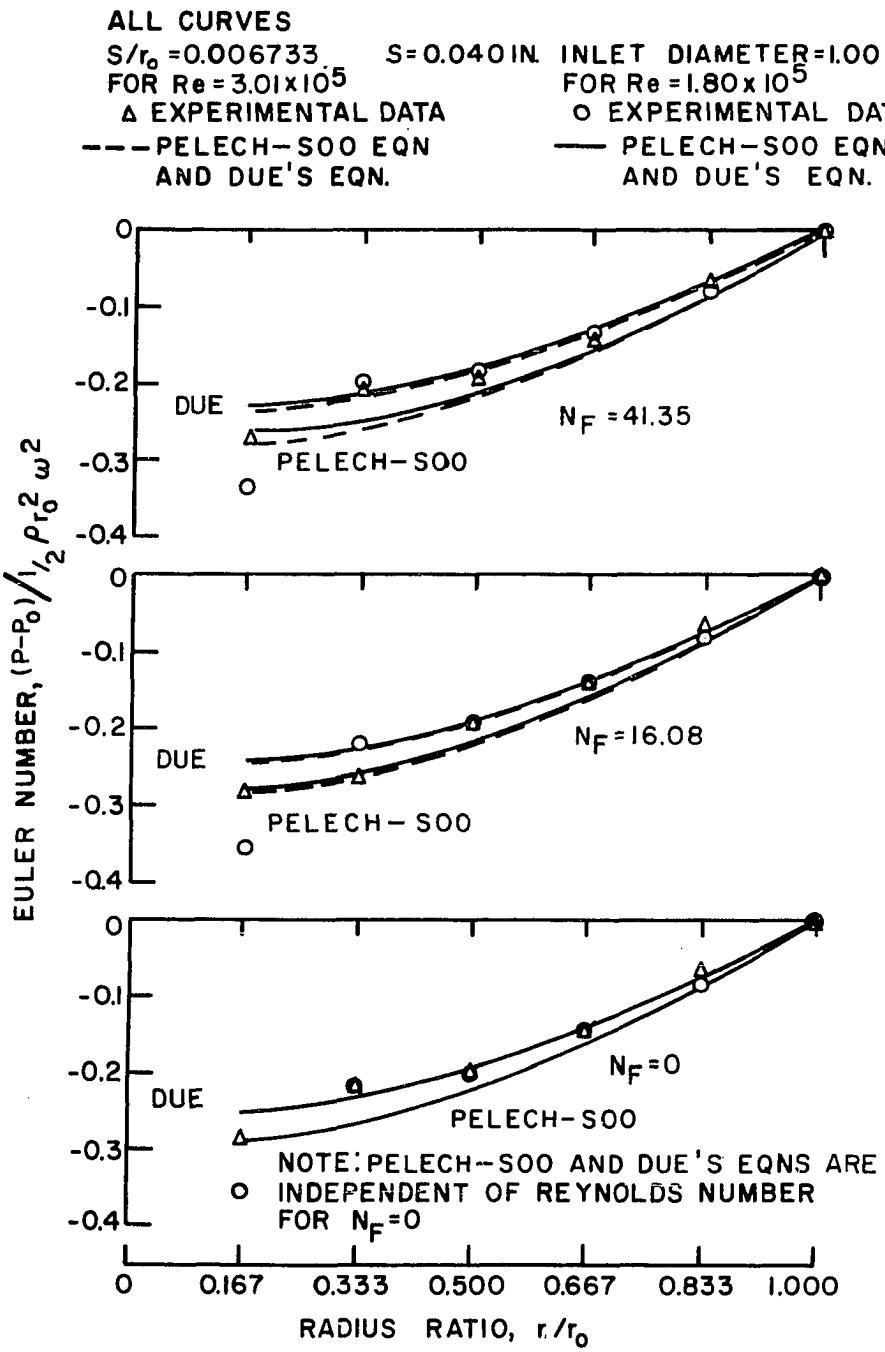
ALL CURVES
S/r0 =0.006733 S=0.040 IN. INLET DIAMETER=1.00 IN.
FOR Re=3.01x10^5
Δ EXPERIMENTAL DATA
--- PELECH-SOO EQN AND DUE'S EQN.
FOR Re=1.80x10^5
o EXPERIMENTAL DATA
— PELECH-SOO EQN. AND DUE'S EQN.
EULER NUMBER, (P-P0)/1/2 ρr0^2 ω^2
0
-0.1
-0.2
-0.3
-0.4
DUE
PELECH-SOO
NF=41.35
NF=16.08
NF=0
NOTE: PELECH-SOO AND DUE'S EQNS ARE INDEPENDENT OF REYNOLDS NUMBER FOR NF=0
0
0.167
0.333
0.500
0.667
0.833
1.000
RADIUS RATIO, r/r0

Figure 9. Plot of Euler number versus radius ratio for gap ratio of 0.004916, comparing experimental values determined using air as a fluid with empirically determined values using water as a fluid (Due, 6) and values calculated from theoretical equations (Pelech and Shapiro, 13; Soo, 17) ($N_F = Q/\nu r_o$)

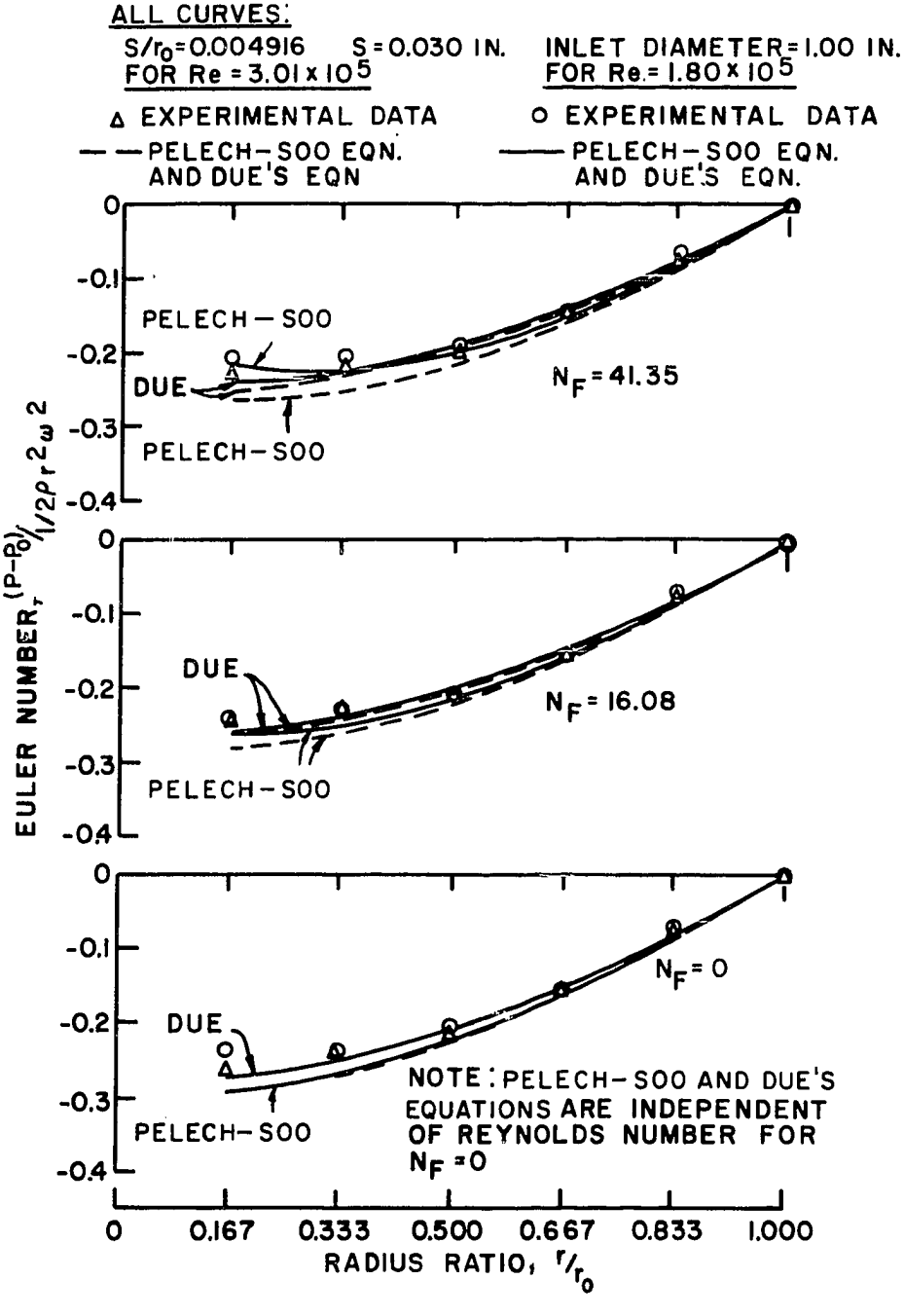
ALL CURVES:
S/r0=0.004916 S=0.030 IN. INLET DIAMETER=1.00 IN.
FOR Re=3.01x10^5 FOR Re.=1.80x10^5
Δ EXPERIMENTAL DATA
o EXPERIMENTAL DATA
— — PELECH-SOO EQN. AND DUE'S EQN
—— PELECH-SOO EQN. AND DUE'S EQN.
EULER NUMBER, (P-P0)/1/2ρr^2ω^2
PELECH-SOO
DUE
PELECH-SOO
N_F=41.35
DUE
PELECH-SOO
N_F=16.08
N_F=0
DUE
PELECH-SOO
NOTE: PELECH-SOO AND DUE'S EQUATIONS ARE INDEPENDENT OF REYNOLDS NUMBER FOR N_F=0
0
-0.1
-0.2
-0.3
-0.4
0 0.167 0.333 0.500 0.667 0.833 1.000
RADIUS RATIO, r/r0

Figure 10. Plot of Euler number versus radius ratio for gap ratio of 0.003333, comparing experimental values determined using air as a fluid with empirically determined values using water as a fluid (Due, 6) and values calculated from theoretical equations (Pelech and Shapiro, 13; Soo, 17) ($N_F = Q/\nu r_o$)

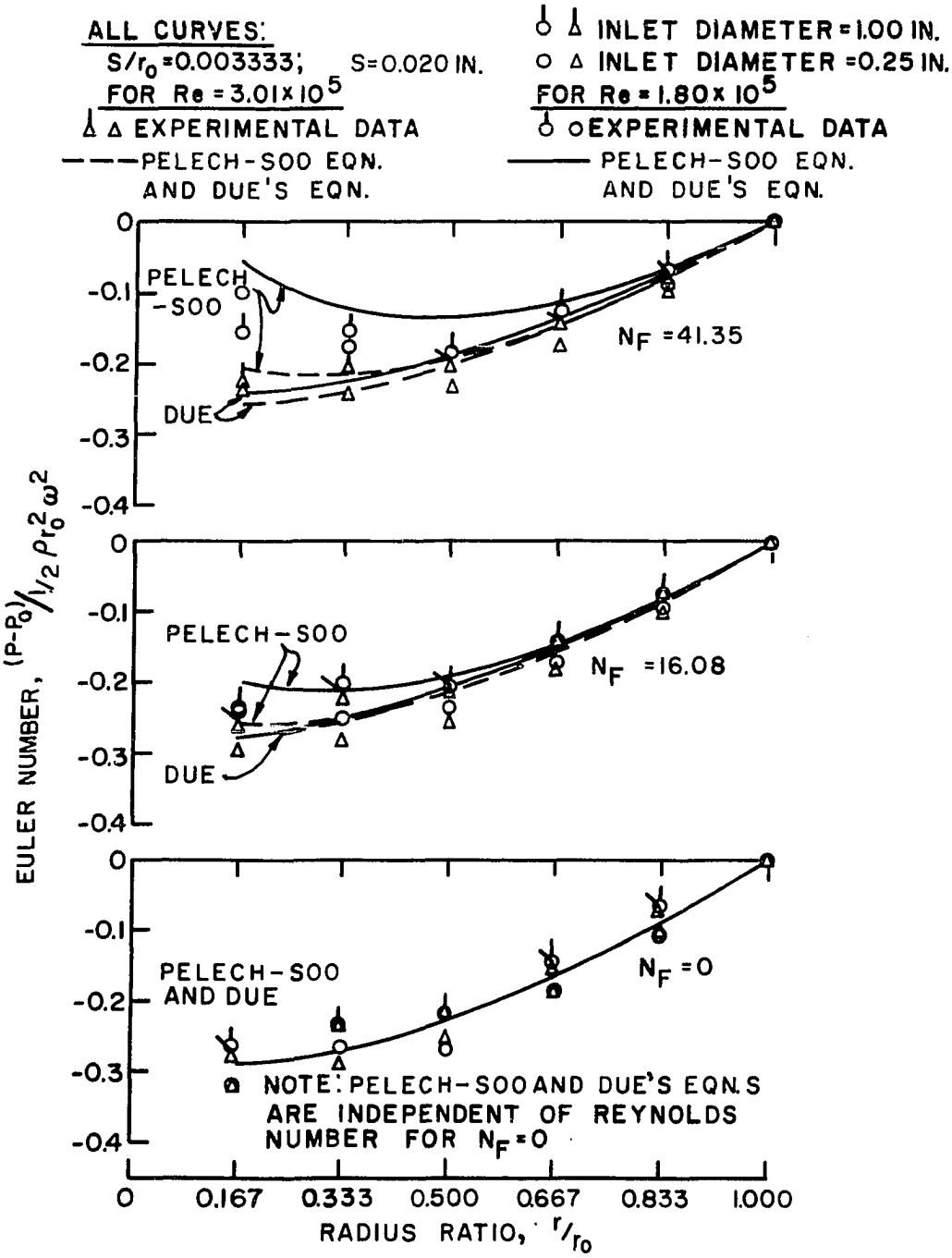
ALL CURVES:
S/r0 = 0.003333; S = 0.020 IN.
FOR Re = 3.01 x 10^5
Δ Δ EXPERIMENTAL DATA
---PELECH-SOO EQN. AND DUE'S EQN.
INLET DIAMETER = 1.00 IN.
INLET DIAMETER = 0.25 IN.
FOR Re = 1.80 x 10^5
o o EXPERIMENTAL DATA
——— PELECH-SOO EQN. AND DUE'S EQN.
PELECH-SOO
DUE
NF = 41.35
NF = 16.08
NF = 0
PELECH-SOO AND DUE
NOTE: PELECH-SOO AND DUE'S EQNS ARE INDEPENDENT OF REYNOLDS NUMBER FOR NF = 0
EULER NUMBER, (P-P0)/1/2 ρ r0^2 ω^2
RADIUS RATIO, r/r0
0
-0.1
-0.2
-0.3
-0.4
0.167
0.333
0.500
0.667
0.833
1.000

Figure 11. Plot of Euler number versus radius ratio for gap ratio of 0.001767, comparing experimental values determined using air as a fluid with empirically determined values using water as a fluid (Due, 6) and values calculated from theoretical equations (Pelech and Shapiro, 13; Soo, 17) ($N_F = Q/\nu r_o$)

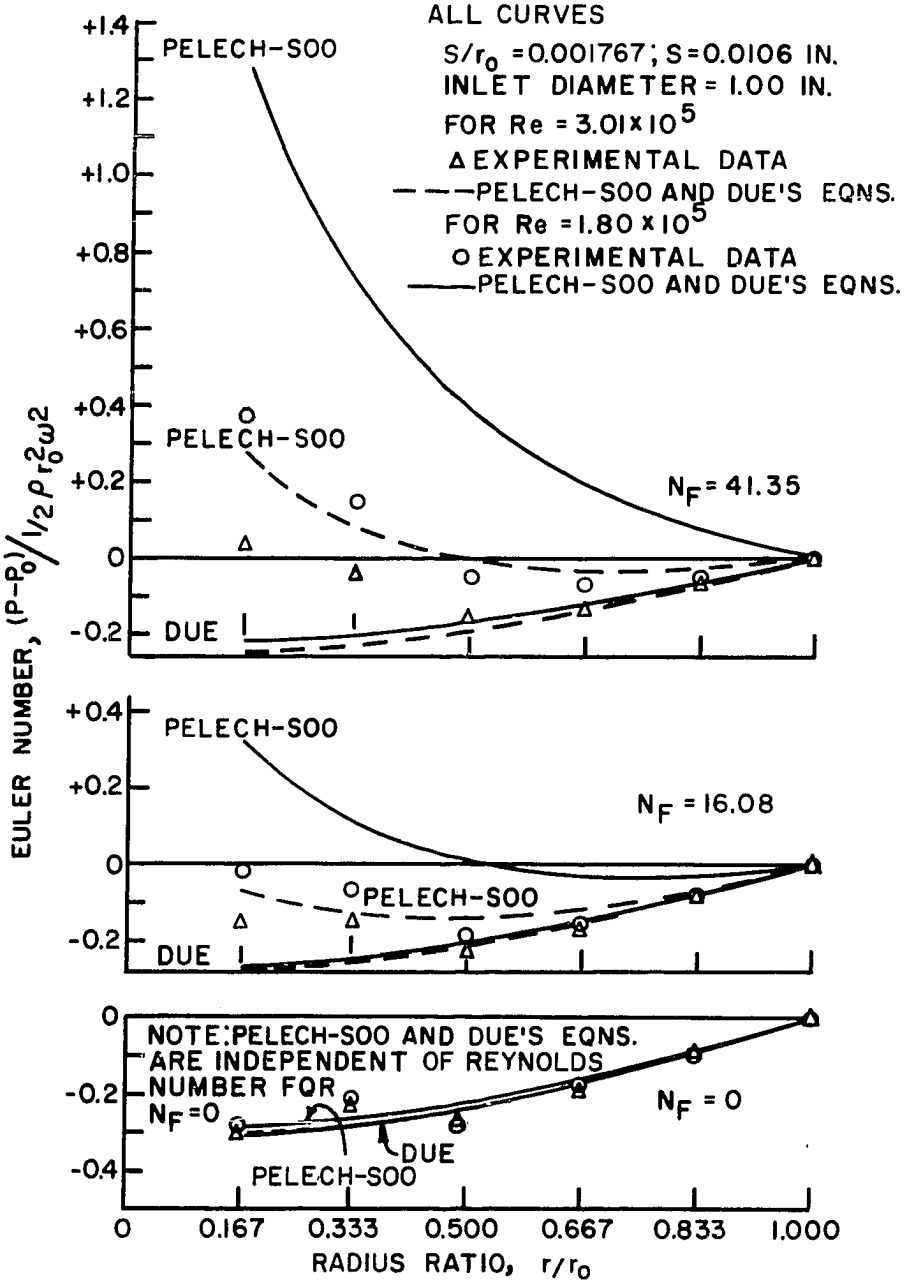
ALL CURVES
S/r0 =0.001767; S=0.0106 IN.
INLET DIAMETER = 1.00 IN.
FOR Re = 3.01×10^5
Δ EXPERIMENTAL DATA
---PELECH-SOO AND DUE'S EQNS.
FOR Re = 1.80×10^5
O EXPERIMENTAL DATA
——PELECH-SOO AND DUE'S EQNS.
PELECH-SOO
PELECH-SOO
DUE
N_F = 41.35
PELECH-SOO
PELECH-SOO
DUE
N_F = 16.08
NOTE: PELECH-SOO AND DUE'S EQNS. ARE INDEPENDENT OF REYNOLDS NUMBER FOR N_F = 0
N_F = 0
DUE
PELECH-SOO
EULER NUMBER, (P-P0)/1/2 ρ r0^2 ω2
+1.4
+1.2
+1.0
+0.8
+0.6
+0.4
+0.2
0
-0.2
-0.4
0
0.167
0.333
0.500
0.667
0.833
1.000
RADIUS RATIO, r/r0

Figure 12. Plot of Euler number versus radius ratio for gap ratio of 0.001583, comparing experimental values determined using air as a fluid with empirically determined values using water as a fluid (Due, 6) and values calculated from theoretical equations (Pelech and Shapiro, 13; Soo, 17) ($N_F = Q/\nu r_o$)

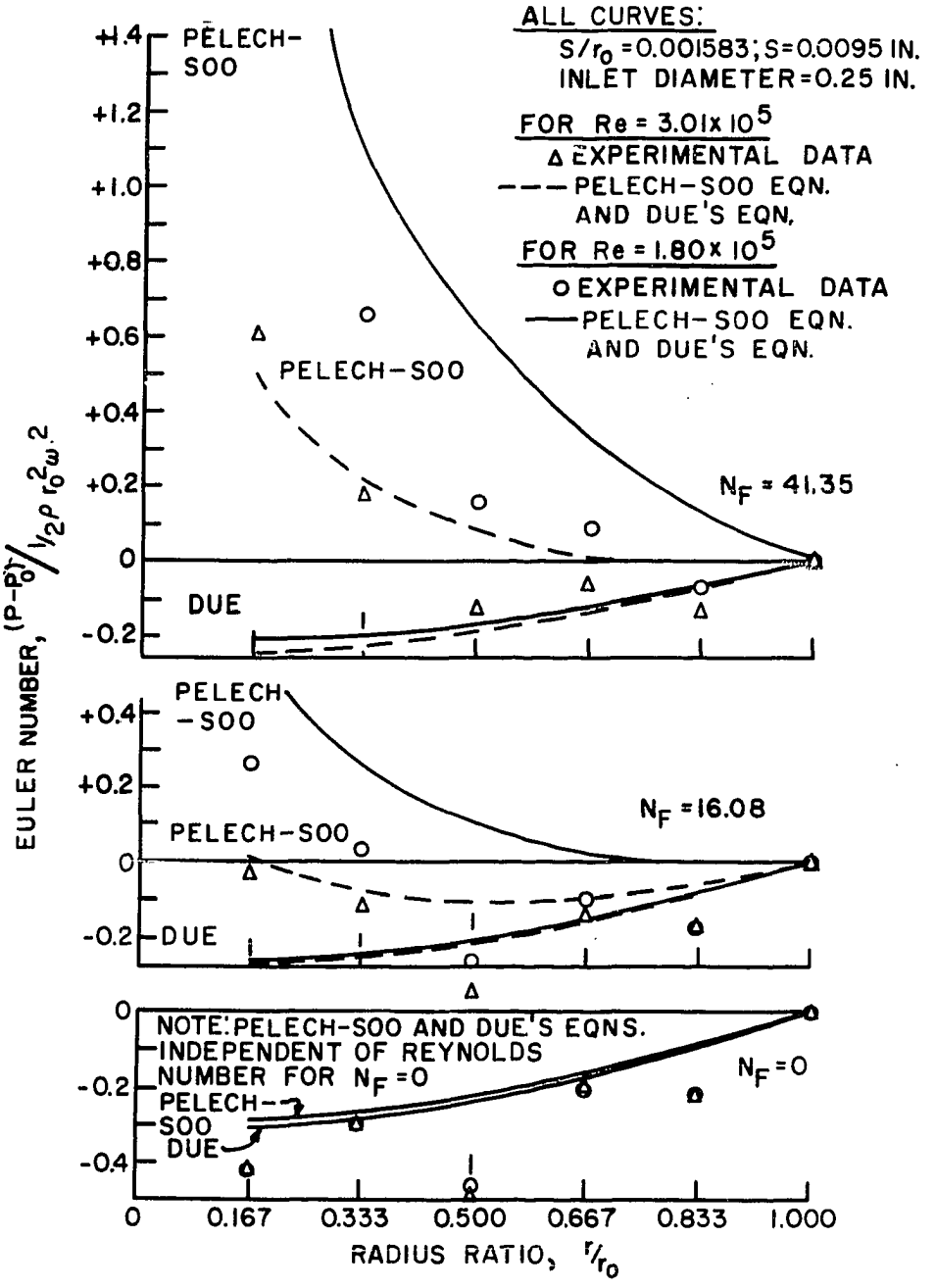
ALL CURVES:
S/r0 = 0.001583; S = 0.0095 IN.
INLET DIAMETER = 0.25 IN.
FOR Re = 3.01 x 10^5
Δ EXPERIMENTAL DATA
--- PELECH-SOO EQN. AND DUE'S EQN.
FOR Re = 1.80 x 10^5
o EXPERIMENTAL DATA
— PELECH-SOO EQN. AND DUE'S EQN.
EULER NUMBER, (P-P0)/½ρ r0²ω²
PELECH-SOO
PELECH-SOO
DUE
NF = 41.35
PELECH-SOO
PELECH-SOO
DUE
NF = 16.08
NOTE: PELECH-SOO AND DUE'S EQNS. INDEPENDENT OF REYNOLDS NUMBER FOR NF = 0
PELECH-SOO
DUE
NF = 0
+1.4
+1.2
+1.0
+0.8
+0.6
+0.4
+0.2
0
-0.2
+0.4
+0.2
0
-0.2
0
-0.2
-0.4
0
0.167
0.333
0.500
0.667
0.833
1.000
RADIUS RATIO, r/r0

Figure 13. Plot of Euler number versus radius ratio for gap ratio of 0.000958, comparing experimental values determined using air as a fluid with empirically determined values using water as a fluid (Due, 6) and values calculated from theoretical equations (Pelech and Shapiro, 13; Soo, 17) ($N_F = Q/\nu r_o$)

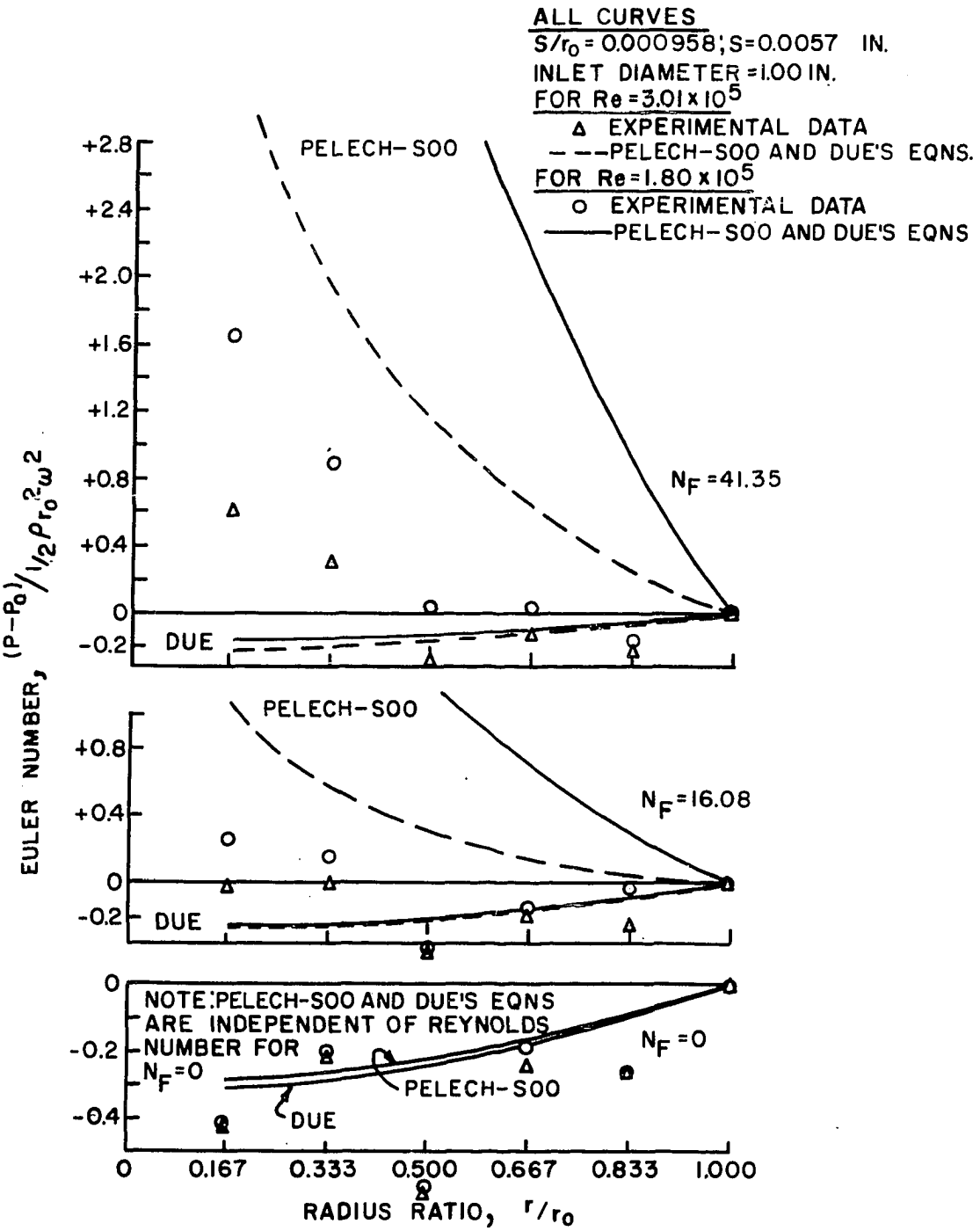
ALL CURVES
S/r0 = 0.000958; S=0.0057 IN.
INLET DIAMETER = 1.00 IN.
FOR Re = 3.01 x 10^5
Δ EXPERIMENTAL DATA
– – – PELECH-SOO AND DUE'S EQNS.
FOR Re = 1.80 x 10^5
o EXPERIMENTAL DATA
—— PELECH-SOO AND DUE'S EQNS
EULER NUMBER, (P-P0)/1/2 ρ r0^2 ω^2
PELECH-SOO
NF = 41.35
DUE
PELECH-SOO
NF = 16.08
DUE
NOTE: PELECH-SOO AND DUE'S EQNS ARE INDEPENDENT OF REYNOLDS NUMBER FOR NF = 0
NF = 0
PELECH-SOO
DUE
+2.8
+2.4
+2.0
+1.6
+1.2
+0.8
+0.4
0
-0.2
-0.4
0.167
0.333
0.500
0.667
0.833
1.000
RADIUS RATIO, r/r0

$$\frac{p-p_o}{\frac{1}{2}\rho\omega^2 r_o^2} = \frac{3}{10}\left[\frac{r^2}{r_o^2} - 1\right] - \frac{12}{\pi}\left[\frac{Q}{s\omega r_o^2}\right]\left[\frac{\nu}{\omega s^2}\right]\ln\left[\frac{r}{r_o}\right] \quad . \qquad (40)$$

Comparison of Equations 38 and 40 reveals that they are identical except for the first term in Equation 38. Euler numbers were calculated from both equations and were found to differ on the order of one percent. Therefore, only one curve was plotted for each set of run conditions and is labelled "Pelech-Soo" in Figures 8 through 13.

The equations developed by Due (6), from test work using water and liquid hydrogen as fluids, are discussed in the Review of Literature section and are repeated below (converted to the notation of this investigation)

$$p-p_o = \frac{1}{2}\rho K^2\omega^2(r^2-r_o^2) \quad , \qquad (41)$$

(for water)

$$K = 0.578 - 4.11\phi - 1.67C \quad , \qquad (42)$$

(for liquid hydrogen)

$$K = 0.906 + 0.012\phi\left(\frac{s}{r_o}\right)^{-1} - 5.36\phi - 51.1\left(\frac{s}{r_o}\right) + 1295.3\left(\frac{s}{r_o}\right)^2 \quad , \qquad (43)$$

where

$$\phi = \left(\frac{1}{r_o\omega}\right)\left(\frac{Q}{2\pi r_o s}\right) \quad . \qquad (44)$$

In Equation 42, C is the gap width in inches. If Equation 41 is appropriately rearranged,

$$\frac{p-p_o}{\frac{1}{2}\rho\omega^2 r_o^2} = K^2\left(\frac{r^2}{r_o^2} - 1\right) \quad . \tag{45}$$

Equations 42, 43 and 45 were used to calculate Euler numbers which were compared to the Euler numbers experimentally determined in this investigation. The Euler numbers calculated using K from Equation 43 were thirty-five percent to several hundred percent smaller than the experimentally determined Euler numbers, thus were not included in Figures 8 through 13. Euler numbers calculated using Equation 42 for K are plotted in Figures 8 through 13 as curves labelled "Due".

Discussion of Experimental Data

Euler numbers were calculated for radius ratios ranging from 0.167 to 1.000 for all combinations of the Reynolds numbers, flow numbers and gap ratios listed in Tables 5, 6 and 7. Preliminary data plots revealed that for the range of any given variable, all of the experimental Euler number profiles were similar. Thus the data trends and agreement or disagreement with values obtained from Equations 38, 40 and 45 could be shown by plotting Euler numbers versus radius ratios for the two extreme Reynolds numbers, the maximum, approximate middle and minimum flow numbers and all of the gap ratios. These

plots are shown in Figures 8 through 13. A discussion of the comparison of experimental data with that calculated from Equation 38 or 40 is included in the Analysis section.

Inspection of Figures 8 and 9 shows that the variation of Reynolds number or flow number within the ranges used in this investigation does not appreciably affect the Euler number profiles for the two largest gap ratios used. Figures 10 through 13 indicate that the influence of the Reynolds number and the flow number is the most evident for radius ratios less than one-half and for the higher flow numbers and the smaller gap ratios. The Euler number increases as either the Reynolds number or the gap ratio decreases or as the flow number increases. For low or zero flow numbers, the Euler number profile appears essentially independent of Reynolds number. These experimental results are consistent with those predicted using either Equation 38 or Equation 40. The last term in either equation may be rearranged into an expression which takes the form: flow number divided by the product of the Reynolds number and the gap ratio. If the flow becomes small or zero, the Euler number in Equations 38 and 40 becomes a function only of radius ratio.

A direct comparison of data taken before and after the inlet hole and pressure tap insert configurations were modified (see the discussion in the Test Program section) is found in Figure 10. Euler numbers calculated from data obtained

after the configurations were modified are smaller by approximately the Euler number uncertainty (0.04) than those calculated from data taken using the original configuration. The form of the Euler number profiles remained the same indicating that the flow pattern apparently had not been changed.

Since the differences in the Euler number magnitudes were approximately the order of the Euler number uncertainty and since the flow patterns were apparently not changed by the modifications, the effects of the modifications will be neglected in this investigation. The effective inlet size is noted on Figures 8 through 13.

Comparison of Experimental Data with Data from the Literature

Inspection of Figures 8 through 13 reveals that the experimental Euler numbers compare very well with those calculated using Equations 42 and 45 (Due, 6) for gap widths of 0.040 inch and 0.030 inch except at the smallest radius ratio where entrance effects may be present. Agreement is also well within the uncertainty limits associated with the Euler numbers for zero throughflow conditions at other gap widths, and for radius ratios greater than 0.50 for all flows except where the experimental Euler number becomes positive. The data used by Due (6) to determine Equation 42 were apparently for throughflows that were low enough that no positive Euler

numbers were developed.

Agreement between experimental Euler numbers and Euler numbers calculated using Equation 38 or 40 was not as good as with Due's (6) data, but was within the uncertainty associated with the experimental Euler numbers for the same conditions as discussed for Due's (6) work. The Euler numbers calculated from Equation 38 or 40 could be positive and had the same form of profile as the experimental Euler numbers, although they were higher than the experimental Euler numbers for all conditions except the 0.040 and 0.030 inch gap widths. The range of flow numbers used in this investigation was apparently such that the low throughflow assumption was not violated for the 0.040 and 0.030 inch gaps.

The agreement of Equation 45 (Due, 6) with Equation 38 or 40 for zero throughflow conditions may be shown by writing out Equation 45 with Equation 42 (in the notation of this investigation) substituted for K.

$$\frac{p-p_o}{\frac{1}{2}\rho r_o^2\omega^2} = \left(\frac{r^2}{r_o^2} - 1\right)\left[0.334 + 16.85\left(\frac{Q}{2\pi r_o^2 s\omega}\right)^2 + 402s^2 - 4.75\left(\frac{Q}{2\pi r_o^2 s\omega}\right) - 164.5s\left(\frac{Q}{2\pi r_o^2 s\omega}\right) - 23.2s\right] \quad (46)$$

If the throughflow, Q, is made zero, Equation 46 becomes

$$\frac{p-p_o}{\frac{1}{2}\rho r_o^2\omega^2} = \left(\frac{r^2}{r_o^2} - 1\right)\left(0.334 + 402s^2 - 23.2s\right) \quad . \tag{47}$$

Equation 47 then agrees with Pelech and Shapiro's (13) or Soo's (17) equation for zero throughflow, which is

$$\frac{p-p_o}{\frac{1}{2}\rho r_o^2\omega^2} = 0.3\left(\frac{r^2}{r_o^2} - 1\right) \quad . \tag{48}$$

Since r is less than r_o, the only positive term in Equation 47 is the last one which is approximately 10^{-2}. The next to last term is even smaller; thus the dominant term is very nearly the same in Equation 47 as the right hand side of Equation 48.

The last two terms in Equation 47 do influence Euler number values for the largest gap ratios. This may be seen by noting that in Figures 8 and 9 the curves from Due's (6) equation have higher values than the Pelech-Soo curves while in Figures 10 through 13 the reverse is true.

ANALYSIS

The calculation or prediction of the radial pressure distribution in the steady, axially symmetric, incompressible, constant viscosity flow of a fluid between a rotating disk and a stationary parallel plate requires a knowledge of the velocity distributions present. (Figure 1 is a sketch of the basic system.) This knowledge can be obtained experimentally by measuring the velocity distributions or by solving the equations governing the fluid flow. The first alternative is extremely difficult in the narrow gaps considered in this investigation. The second alternative is considered in the following analysis which examines the governing equations.

The governing equations assumed to be appropriate for this flow problem are the Navier-Stokes equations and the continuity equation written in cylindrical coordinates. These equations are

$$\rho\left[u\frac{\partial u}{\partial r} + \frac{v}{r}\frac{\partial u}{\partial \theta} - \frac{v^2}{r} + w\frac{\partial u}{\partial z}\right]$$

$$= F_r - \frac{\partial p}{\partial r} + \mu\left[\frac{\partial^2 u}{\partial r^2} + \frac{1}{r}\frac{\partial u}{\partial r} - \frac{u}{r^2} + \frac{1}{r^2}\frac{\partial^2 u}{\partial \theta^2} - \frac{2}{r^3}\frac{\partial v}{\partial \theta} + \frac{\partial^2 u}{\partial z^2}\right] \qquad (49)$$

$$\rho\left[u\frac{\partial v}{\partial r} + \frac{v}{r}\frac{\partial v}{\partial \theta} + \frac{uv}{r} + w\frac{\partial v}{\partial z}\right]$$

$$= F_\theta - \frac{1}{r}\frac{\partial p}{\partial \theta} + \mu\left[\frac{\partial^2 v}{\partial r^2} + \frac{1}{r}\frac{\partial v}{\partial r} - \frac{v}{r^2} + \frac{1}{r^2}\frac{\partial^2 v}{\partial \theta^2} + \frac{2}{r^2}\frac{\partial u}{\partial \theta} + \frac{\partial^2 v}{\partial z^2}\right] \quad (50)$$

$$\rho\left[u\frac{\partial w}{\partial r} + \frac{v}{r}\frac{\partial w}{\partial \theta} + w\frac{\partial w}{\partial z}\right]$$

$$= F_z - \frac{\partial p}{\partial z} + \mu\left[\frac{\partial^2 w}{\partial r^2} + \frac{1}{r}\frac{\partial w}{\partial r} + \frac{1}{r^2}\frac{\partial^2 w}{\partial \theta^2} + \frac{\partial^2 w}{\partial z^2}\right] \quad (51)$$

$$\frac{1}{r}\frac{\partial (ru)}{\partial r} + \frac{1}{r}\frac{\partial v}{\partial \theta} + \frac{\partial w}{\partial z} = 0 \quad . \quad (52)$$

Even though it is recognized that they are not independent, it is convenient in the following order of magnitude analysis to represent the radial velocity, u, as the sum of two components. One component, u_1, is the result of the centrifugal action and the other, u_2, depends on the net throughflow. This may be expressed in equation form as

$$u = u_1 + u_2 \quad (53)$$

where u_1 and u_2 are due to the centrifugal effect and the net throughflow, respectively.

The body forces F_r, F_θ and F_z may be neglected compared to other fluid forces and all derivatives with respect to θ may be set to zero as a result of the assumed axial symmetry. If u is replaced by $u_1 + u_2$ and the previous assumptions applied, Equations 49 through 52 may be rewritten, with some rearranging, as

$$\overbrace{u_1\frac{\partial u_1}{\partial r} + w\frac{\partial u_1}{\partial z}}^{\text{I}} - \overbrace{\frac{v^2}{r}}^{\text{II}} + \overbrace{u_1\frac{\partial u_2}{\partial r} + u_2\frac{\partial u_1}{\partial r} + w\frac{\partial u_2}{\partial z}}^{\text{III}} + \overbrace{u_2\frac{\partial u_2}{\partial r}}^{\text{IV}}$$

$$= -\frac{1}{\rho}\frac{\partial p}{\partial r} + \nu\left[\overbrace{\frac{\partial^2 u_1}{\partial r^2} + \frac{1}{r}\frac{\partial u_1}{\partial r} - \frac{u_1}{r^2} + \frac{\partial^2 u_2}{\partial r^2} + \frac{1}{r}\frac{\partial u_2}{\partial r} - \frac{u_2}{r^2}}^{\text{V}} + \overbrace{\frac{\partial^2 u_1}{\partial z^2} + \frac{\partial^2 u_2}{\partial z^2}}^{\text{VI}}\right]$$

(54)

$$\overbrace{u_1\frac{\partial v}{\partial r} + \frac{u_1 v}{r} + w\frac{\partial v}{\partial z}}^{\text{I}} + \overbrace{u_2\frac{\partial v}{\partial r} + \frac{u_2 v}{r}}^{\text{III}} = \nu\left[\overbrace{\frac{\partial^2 v}{\partial r^2} + \frac{1}{r}\frac{\partial v}{\partial r} - \frac{v}{r^2}}^{\text{V}} + \overbrace{\frac{\partial^2 v}{\partial z^2}}^{\text{VI}}\right]$$

(55)

$$\overbrace{u_1\frac{\partial w}{\partial r} + w\frac{\partial w}{\partial z}}^{\text{I}} + \overbrace{u_2\frac{\partial w}{\partial r}}^{\text{III}} = -\frac{1}{\rho}\frac{\partial p}{\partial z} + \nu\left[\overbrace{\frac{\partial^2 w}{\partial r^2} + \frac{1}{r}\frac{\partial w}{\partial r}}^{\text{V}} + \overbrace{\frac{\partial^2 w}{\partial z^2}}^{\text{VI}}\right] \tag{56}$$

$$\frac{1}{r}\frac{\partial (ru_1)}{\partial r} + \frac{1}{r}\frac{\partial (ru_2)}{\partial r} + \frac{\partial w}{\partial z} = 0 \quad . \tag{57}$$

The following boundary conditions apply for this problem. For r>0

$$u_1(r,0) = 0 \tag{58}$$

$$u_1(r,s) = 0 \tag{59}$$

$$v(r,0) = r\omega \tag{60}$$

$$v(r,s) = 0 \tag{61}$$

$$w(r,0) = 0 \tag{62}$$

$$w(r,s) = 0 \tag{63}$$

$$\int_0^s 2\pi r u_2 dz = Q \quad . \tag{64}$$

The Roman numerals shown above Equations 54, 55 and 56 will be used in the following text and tables for identifying the various groupings of terms in the equations. Table 8 lists

the group number and the physical significance of each group.

Table 8. Group numbers and corresponding fluid terms

Group No.	Type of fluid terms
I	Convective terms related only to centrifugal effects
II	Centrifugal force term
III	Convective terms related to both centrifugal and throughflow effects
IV	Convective term related only to throughflow effects
V	Viscous terms due to velocity variation in the r direction
VI	Viscous terms due to velocity variation in the z direction

The technique utilized for determining the relative importance of the different terms in Equations 54, 55 and 56 is described by Kline (9). The domain of interest for this problem is the volume between the rotating disk and the stationary plate from an inner radius greater than zero to the disk outer radius. The requirement for the inner radius to be greater than zero arises not only from the fact that certain terms in Equations 54 through 56 would be infinite for r=0, but also from the practical consideration of supplying fluid to the gap at the center of the rotating disk. In addition,

the transition from the inlet hole to the gap volume is an orifice having a cross-section area of πsd where d is the diameter of the inlet hole. The fluid flow for some distance downstream is affected by the entrance conditions. The entrance effects are not included in this analysis and their extent was not determined. No information on entrance effects for the configuration used in this investigation was found in the literature. Thus the domain of interest for this analysis is the volume between the rotating disk and the stationary plate from the smallest radius at which no entrance effects are found to the outer radius of the disk.

The following dimensionless variables are defined in the domain

$$R = \frac{r}{r_o} \qquad 0<r\leq r_o \tag{65}$$

$$Z = \frac{z}{s} \qquad 0<z\leq s \tag{66}$$

$$V = \frac{v}{r_o\omega} \qquad 0\leq v\leq r\omega \ , \quad 0<r\leq r_o \tag{67}$$

$$U_1 = \left(\frac{u_1}{r_o\omega}\right)\left(\frac{\nu}{\omega s^2}\right) \tag{68}$$

$$U_2 = \frac{u_2}{\frac{Q}{2\pi r_i s}} \tag{69}$$

$$W = \left(\frac{w}{s\omega}\right)\left(\frac{\nu}{\omega s^2}\right) \tag{70}$$

$$P = \frac{p}{\rho r_o^2 \omega^2} \quad . \tag{71}$$

The dimensionless parameters U_1 and W may be shown to be of approximate magnitude 1 as follows. If the velocities u_1 and w are smooth and well behaved, and the variables r and z are taken to be approximately the same magnitude as r_o and s, then $\frac{\partial(\ )}{\partial r}$ and $\frac{\partial(\ )}{\partial z}$ are approximately the same magnitude as $\frac{(\ )}{r_o}$ and $\frac{(\ )}{s}$.

The approximate magnitude of u_1 may be determined by considering Equation 54 for the condition of zero throughflow (i.e., $u_2 = 0$). It will be shown later that all viscous terms except $\frac{\partial^2 u_1}{\partial z^2}$ may be neglected on a magnitude basis. The test results in Figures 8 through 13 show that at least for magnitude purposes, the pressure may be considered as a constant. If the inertial terms in the r direction are assumed small (i.e., $u_1\frac{\partial u_1}{\partial r}$ and $w\frac{\partial u_1}{\partial r} \sim 0$), then Equation 54 (for magnitude comparison purposes) becomes

$$\frac{v^2}{r} \sim \nu\frac{\partial^2 u_1}{\partial z^2} \quad . \tag{54-A}$$

Then if $v \sim r_o\omega$, $r \sim r_o$;

$$\frac{r_o^2\omega^2}{r} \sim \nu\frac{u_1}{s^2} \tag{54-B}$$

and, if rearranged

$$\left(\frac{u_1}{r_o\omega}\right)\left(\frac{\nu}{\omega s^2}\right) \sim 1 \quad . \tag{54-C}$$

If equation 57 is written for the same conditions

$$\frac{1}{r}\frac{\partial(ru_1)}{\partial r} = -\frac{\partial w}{\partial z} \quad . \tag{57-A}$$

If the appropriate magnitudes are substituted into 57-A,

$$\frac{r_o u_1}{r_o^2} \sim \frac{w}{s} \qquad \text{or} \qquad u \sim \frac{r_o}{s} w \quad . \tag{57-B}$$

Then substituting 57-B into 54-C,

$$\left(\frac{w}{s\omega}\right)\left(\frac{\nu}{\omega s^2}\right) \sim 1 \quad . \tag{57-C}$$

The r_i included in 69 is some characteristic radius to be defined later. Thus U_2 represents the ratio of the radial throughflow component of velocity at a point in the gap to the average throughflow velocity at some characteristic radius. Dimensionless variables 65, 66 and 67 vary from zero to one. Dimensionless variable 71 is the ratio of the pressure to a term which may be considered to be the pressure due to centrifugal action alone. As the magnitude of the pressure will in general depend on the convective terms and the viscous terms in addition to the centrifugal terms, no reliable estimate of the range of values of the dimensionless pressure, P, can be

made. This does not hinder the check of the importance of the other terms since the pressure is the dependent variable in this investigation.

In summary, the dimensionless variables 65 through 70 vary over approximately the same range, and thus may be used as reference magnitudes of approximate value 1. The dimensionless velocities are assumed to be well behaved and have no abrupt changes in value so that in the domain of interest, the magnitude of differentials such as $\frac{\partial(\ )}{\partial R}$ or $\frac{\partial(\ )}{\partial Z}$ may be taken as $\frac{(\ )}{R}$ or $\frac{(\ )}{Z}$, respectively.

If the dimensionless variables 65 through 71 are substituted into Equations 54, 55 and 56 and the resulting equations made dimensionless, the following equations will be obtained

$$\overset{\text{I}}{\overbrace{\left(\frac{\omega s^2}{\nu}\right)^2\left[U_1\frac{\partial U_1}{\partial R}+W\frac{\partial U_1}{\partial Z}\right]}}-\overset{\text{II}}{\overbrace{\frac{V^2}{R}}}$$

$$+\left(\frac{\omega s^2}{\nu}\right)\left(\frac{1}{r_o\omega}\right)\left(\frac{Q}{2\pi r_i s}\right)\overset{\text{III}}{\overbrace{\left[U_1\frac{\partial U_2}{\partial R}+U_2\frac{\partial U_1}{\partial R}+\left(\frac{s}{r_o}\right)W\frac{\partial U_2}{\partial R}\right]}}$$

$$+\left(\frac{1}{r_o\omega}\right)^2\left(\frac{Q}{2\pi r_i s}\right)^2\overset{\text{IV}}{\overbrace{\left[U_2\frac{\partial U_2}{\partial R}\right]}}=\frac{\partial P}{\partial R}+\left(\frac{\nu}{r_o^2\omega}\right)\left(\frac{\omega s^2}{\nu}\right)\overset{\text{V-A}}{\overbrace{\left[\frac{\partial^2 U_1}{\partial R^2}+\frac{1}{R}\frac{\partial U_1}{\partial R}-\frac{U_1}{R^2}\right]}}$$

$$+ \left(\frac{\nu}{r_o^2\omega}\right)\left(\frac{1}{r_o\omega}\right)\left(\frac{Q}{2\pi r_i s}\right)\left[\overset{\text{V-B}}{\overbrace{\frac{\partial^2 U_2}{\partial R^2} + \frac{1}{R}\frac{\partial U_2}{\partial R} - \frac{U_2}{R^2}}}\right] + \left[\overset{\text{VI-A}}{\overbrace{\frac{\partial^2 U_1}{\partial Z^2}}}\right]$$

$$+ \left(\frac{\nu}{s^2\omega}\right)\left(\frac{1}{r_o\omega}\right)\left(\frac{Q}{2\pi r_i s}\right)\left[\overset{\text{VI-B}}{\overbrace{\frac{\partial^2 U_2}{\partial Z^2}}}\right] \tag{72}$$

$$\left(\frac{\omega s^2}{\nu}\right)\left[\overset{\text{I}}{\overbrace{U_1\frac{\partial V}{\partial R} + \frac{U_1 V}{R} + W\frac{\partial V}{\partial Z}}}\right] + \left(\frac{1}{r_o\omega}\right)\left(\frac{Q}{2\pi r_i s}\right)\left[\overset{\text{III}}{\overbrace{U_2\frac{\partial V}{\partial R} + \frac{U_2 V}{R}}}\right]$$

$$= \left(\frac{\nu}{\omega r_o^2}\right)\left[\overset{\text{V}}{\overbrace{\frac{\partial^2 V}{\partial R^2} + \frac{1}{R}\frac{\partial V}{\partial R} - \frac{V}{R^2}}}\right] + \frac{\nu}{\omega s^2}\left[\overset{\text{VI}}{\overbrace{\frac{\partial^2 V}{\partial Z^2}}}\right] \tag{73}$$

$$\left(\frac{s}{r_o}\right)^2\left(\frac{\omega s^2}{\nu}\right)^2\left[\overset{\text{I}}{\overbrace{U_1\frac{\partial W}{\partial R} + W\frac{\partial W}{\partial Z}}}\right] + \left(\frac{s}{r_o}\right)^2\left(\frac{\omega s^2}{\nu}\right)\left(\frac{1}{r_o\omega}\right)\left(\frac{Q}{2\pi r_i s}\right)\left[\overset{\text{III}}{\overbrace{U_2\frac{\partial W}{\partial R}}}\right]$$

$$= -\frac{\partial P}{\partial Z} + \left(\frac{s}{r_o}\right)^2\left(\frac{\nu}{r_o^2\omega}\right)\left(\frac{\omega s^2}{\nu}\right)\left[\overset{\text{V}}{\overbrace{\frac{\partial^2 W}{\partial R^2} + \frac{1}{R}\frac{\partial W}{\partial R}}}\right] + \left(\frac{s}{r_o}\right)^2\left[\overset{\text{VI}}{\overbrace{\frac{\partial^2 W}{\partial Z^2}}}\right] \tag{74}$$

Groups V and VI in Equations 73 and 74 correspond to terms

V-A and VI-A in Equation 72.

The magnitudes of terms in Equation 73 differ from their counterparts in Equation 72 by a factor of $\frac{\omega s^2}{\nu}$. If $\frac{\omega s^2}{\nu}$ is less than 1, the corresponding terms in Equation 73 are larger. If $\frac{\omega s^2}{\nu}$ is less than one, the corresponding terms in Equation 73 are smaller by a factor of $\frac{\omega s^2}{\nu}$.

The magnitudes of each term in Equation 74 are smaller by $\left(\frac{s}{r_o}\right)^2$ than the corresponding terms in Equation 72. Also the third term in Group III of Equation 72 is smaller than the other two terms in the group. Since $\frac{s}{r_o} \sim 10^{-3}$ for the gap range specified in this investigation these terms may be neglected in subsequent analysis.

If the terms in Equation 74 are taken as negligible when compared to corresponding terms in Equation 72, then it follows that $\frac{\partial p}{\partial z}$ is negligible compared to $\frac{\partial p}{\partial r}$.

The terms in Group V may also be neglected in comparison with those in Group VI since the ratio of the magnitudes of the Group V terms to the Group VI terms is approximately $\left(\frac{s}{r_o}\right)^2$.

If the terms discussed previously are neglected, Equations 54, 55 and 56 may be rewritten as

$$\overbrace{u_1\frac{\partial u_1}{\partial r} + w\frac{\partial u_1}{\partial z}}^{\text{I}} \overbrace{- \frac{v^2}{r}}^{\text{II}} + \overbrace{u_1\frac{\partial u_2}{\partial r} + u_2\frac{\partial u_1}{\partial r}}^{\text{III}} + \overbrace{u_2\frac{\partial u_2}{\partial r}}^{\text{IV}} = -\frac{1}{\rho}\frac{\partial p}{\partial r} + \overbrace{\nu\frac{\partial^2 u_1}{\partial z^2}}^{\text{VI-A}} + \overbrace{\nu\frac{\partial^2 u_2}{\partial z^2}}^{\text{VI-B}} \qquad (75)$$

$$\overbrace{u_1\frac{\partial v}{\partial r} + \frac{u_1 v}{r} + w\frac{\partial v}{\partial z}}^{\text{I}} + \overbrace{u_2\frac{\partial v}{\partial r} + \frac{u_2 v}{r}}^{\text{III}} = \overbrace{\frac{\partial^2 v}{\partial z^2}}^{\text{VI}} \qquad (76)$$

$$\frac{\partial p}{\partial z} = 0 \qquad (77)$$

The dimensionless parameters associated with the magnitudes of the terms in Equations 75, 76 and 77 are listed in Table 9 along with the associated terms and group numbers. The dimensionless parameters involving the throughflow rate are also presented in terms of N_F as used in the experimental portion of this investigation.

The numerator of the dimensionless parameter, $\frac{\omega s^2}{\nu}$, represents a centrifugal force per unit volume at the disk outer radius and the denominator represents a viscous force per unit volume related to the tangential velocity gradient across the gap width at the same location. The dimensionless parameter $\frac{\omega r_o^2}{\nu}$ represents the ratio of centrifugal force per unit volume to viscous force per unit volume (related to the velocity gradient $\frac{r_o \omega}{r_o}$) at the disk outer radius.

If the inertia forces are greater than the viscous forces (i.e., $\frac{\omega s^2}{\nu} >> 1$, >> implies much greater), the centrifugal force term and the viscous terms concerning u_1 and v in Equations 75 and 76 may be neglected in the flow analysis. Whether the viscous term involving u_2 in Equation 75 may be

Table 9. Summary of dimensionless parameters associated with terms in Equations 75, 76 and 77

Dimensionless parameter or magnitude	Group No.	Associated terms
$\left(\frac{\omega s^2}{\nu}\right)^2$	I	$u_1\frac{\partial u_1}{\partial r}$, $w\frac{\partial u_1}{\partial z}$
1	II, VI-A	$\frac{v^2}{r}$, $\frac{\partial^2 u_1}{\partial z^2}$
$\left[\left(\frac{\omega s^2}{\nu}\right)\left(\frac{1}{r_o\omega}\right)\left(\frac{Q}{2\pi r_i s}\right)\right]$ or $\left[\left(\frac{1}{2\pi}\right)\left(\frac{s}{r_i}\right)(N_F)\right]$	III	$u_1\frac{\partial u_2}{\partial r}$, $u_2\frac{\partial u_1}{\partial r}$
$\left[\left(\frac{1}{r_o\omega}\right)^2\left(\frac{Q}{2\pi r_i s}\right)^2\right]$ or $\left[\left(\frac{\omega s^2}{\nu}\right)^{-2}\left(\frac{s}{r_i}\right)^2\left(\frac{1}{2\pi}\right)^2(N_F)^2\right]$	IV	$u_2\frac{\partial u_2}{\partial r}$
$\left[\left(\frac{\omega s^2}{\nu}\right)^{-1}\left(\frac{1}{r_o\omega}\right)\left(\frac{Q}{2\pi r_i s}\right)\right]$ or $\left[\left(\frac{\omega s^2}{\nu}\right)^{-2}\left(\frac{1}{2\pi}\right)\left(\frac{s}{r_i}\right)(N_F)\right]$	VI-B	$\frac{\partial^2 u_2}{\partial z^2}$
$\left(\frac{\omega s^2}{\nu}\right)$	I	$u_1\frac{\partial v}{\partial r}$, $\frac{u_1 v}{r}$, $w\frac{\partial v}{\partial z}$
$\left[\left(\frac{1}{r_o\omega}\right)\left(\frac{Q}{2\pi r_i s}\right)\right]$ or $\left[\left(\frac{\omega s^2}{\nu}\right)^{-1}\left(\frac{1}{2\pi}\right)\left(\frac{s}{r_i}\right)(N_F)\right]$	III	$u_2\frac{\partial v}{\partial r}$, $\frac{u_2 v}{r}$
$\left(\frac{\omega s^2}{\nu}\right)^{-1}$	VI	$\frac{\partial^2 v}{\partial z^2}$

neglected or not depends on the magnitude of $\left(\frac{1}{r_o\omega}\right)\left(\frac{Q}{2\pi r_i s}\right)$ compared to $\left(\frac{\omega s^2}{\nu}\right)^{-1}$. If the magnitudes are such that $\left[\left(\frac{\omega s^2}{\nu}\right)^{-1}\left(\frac{1}{r_o\omega}\right)\left(\frac{Q}{2\pi r_i s}\right)\right]$ is large compared to 1, then $\frac{\partial^2 u_2}{\partial z^2}$ may not be neglected. Conversely, if $\frac{\omega s^2}{\nu} << 1$, which usually implies flow of a highly viscous nature, the viscous and centrifugal terms are important and the convective terms may be neglected.

The importance of the throughflow effects is related to the relative magnitudes of $\left[\left(\frac{1}{r_o\omega}\right)\left(\frac{Q}{2\pi r_i s}\right)\right]$ (indicated as N_V in the remainder of this section) and $\frac{\omega s^2}{\nu}$. One interpretation of the physical significance of N_V is that it represents the ratio of the local average throughflow velocity to the tangential velocity of the disk outer radius. Another interpretation may be obtained by rearranging the variables in N_V as follows

$$N_V = \left[\left(\frac{1}{r_o\omega}\right)\left(\frac{Q}{2\pi r_i s}\right)\right] = \left[\left(\frac{1}{2\pi}\right)\left(\frac{\nu}{\omega s^2}\right)\left(\frac{s}{r_i}\right)\left(\frac{Q}{\nu r_o}\right)\right] , \qquad (78)$$

where

$$N_F = \frac{Q}{\nu r_o} .$$

The right hand side of Equation 78 now represents the ratio of the local force due to throughflow to the centrifugal force at the disk outer diameter. The dimensionless parameter N_F was used in the experimental work in this investigation and

may be thought of as being the ratio of fluid forces due to throughflow to fluid forces due to viscous effects.

If N_v is much larger than $\frac{\omega s^2}{\nu}$ and 1, the terms in Groups III and IV dominate the analysis. The importance of the centrifugal force term and the viscous force terms depends on the relative magnitudes of N_v, 1 and $\left(\frac{\omega s^2}{\nu}\right)^{-1}$. If $\frac{\omega s^2}{\nu}$ is much larger than N_v, the terms related to the throughflow may be neglected and the importance of the centrifugal force and viscous terms depends on the relative values of $\frac{\omega s^2}{\nu}$, $\left(\frac{\omega s^2}{\nu}\right)^{-1}$ and 1.

These results substantiate the results of the order of magnitude analysis presented in Pelech and Shapiro (13) or Pelech (12).

Tables 10 and 11 show maximum and minimum values of N_v for each gap width, N_F, $\frac{\omega s^2}{\nu}$ and the extreme values of the Reynolds numbers. The values of N_v were calculated at the radii corresponding to the innermost and outermost pressure taps.

Verification of the importance of the dimensionless parameters listed in Table 9 may be obtained by comparing experimental data with theoretical data calculated from Pelech and Shapiro's (13) or Soo's (17) equations. Both equations assumed values of $\frac{\omega s^2}{\nu}$ and Q to be very nearly zero in determining equations for u, v and w. These assumptions and appropriate manipulations (described in the Review of

Table 10. Values of $\frac{\omega s^2}{\nu}$ and N_V for test runs made with a Reynolds number of 3.01×10^5

Gap width (inch)	$\frac{\omega s^2}{\nu}$	$\frac{\nu}{\omega s^2}$	$N_F = 41.35$		$N_F = 16.08$	
			Maximum N_V	Minimum N_V	Maximum N_V	Minimum N_V
0.0400	13.63	0.0734	0.1182	0.0197	0.0455	0.0076
0.0300	7.27	0.1385	0.1578	0.0263	0.0606	0.0101
0.0200	3.34	0.3000	0.2364	0.0394	0.0906	0.0151
0.0106	0.94	1.0650	0.4458	0.0743	0.1716	0.0286
0.0095	0.75	1.3340	0.4850	0.0808	0.1866	0.0311
0.00575	0.28	3.570	0.8220	0.1370	0.3160	0.0527

Table 11. Values of $\frac{\omega s^2}{\nu}$ and N_V for test runs made with a Reynolds number of 1.80×10^5

Gap width (inch)	$\frac{\omega s^2}{\nu}$	$\frac{\nu}{\omega s^2}$	$N_F = 41.35$		$N_F = 16.08$	
			Maximum N_V	Minimum N_V	Maximum N_V	Minimum N_V
0.0400	8.17	0.1225	0.1974	0.0329	0.0756	0.0126
0.0300	4.36	0.2290	0.2628	0.0438	0.1008	0.0168
0.0200	2.00	0.5000	0.3948	0.0658	0.1518	0.0253
0.0106	0.56	1.7850	0.7440	0.1240	0.2856	0.0476
0.0095	0.45	2.2250	0.8100	0.1350	0.3114	0.0519
0.00575	0.17	5.8800	1.3740	0.2290	0.5274	0.0879

Literature section) allowed closed form equations to be determined by considering only the $\frac{v^2}{r}$ term and the $\frac{\partial^2 u}{\partial z^2}$ term. The velocity equations thus determined were substituted into Equation 1 by Soo (17) or into Equation 1 less the $u\frac{\partial u}{\partial r}$ and $w\frac{\partial u}{\partial z}$ terms by Pelech and Shapiro (13) to obtain an expression for the pressure gradient in the radial direction. This expression was integrated from r_o to r (r>0), then rearranged to give an equation for the Euler number. Euler numbers were calculated from the theoretically determined equation for each radius where the pressure was measured. The theoretical Euler numbers are compared to the experimentally determined Euler numbers in Figures 8 through 13. The comparison of experimental, theoretical and empirical Euler numbers developed from Due's (6) work has been discussed in the Results section. The following discussion will examine the agreement of experimental and theoretical data as related to the dimensionless terms listed in Table 9.

Examination of Tables 10 and 11 reveals that the maximum difference in relative magnitude of the dimensionless parameters listed never exceeded 1000, with the differences mostly on the order of 100 to 10. Thus no group of terms, or associated effects, from Equations 75, 76 or 77 greatly dominated the fluid flow. No experimental data were taken under the conditions assumed by Pelech and Shapiro (13) or Soo (17) (i.e., $\left(\frac{\omega s^2}{\nu}\right)^{-1} >> \frac{\omega s^2}{\nu}$, N_v or $N_v^2\left(\frac{\omega s^2}{\nu}\right)^{-1}$); thus the general

lack of agreement between the experimental and the theoretical data could be expected.

The dimensionless term $\frac{\omega s^2}{\nu}$ was larger than the other dimensionless parameters by factors ranging from 100 to 1000 for the 0.040, 0.030 and 0.020 inch gap runs. The magnitude of $\left(\frac{\omega s^2}{\nu}\right)^{-1}$ was approximately the same as that of N_V. For these runs, the Group I terms (convective terms related to centrifugal action) were the most important and apparently influenced the flow so that the experimental Euler numbers were larger than the theoretical Euler numbers.

For the remaining gap widths, $\frac{\omega s^2}{\nu}$ was approximately equal to, or at least one-tenth of, $\left(\frac{\omega s^2}{\nu}\right)^{-1}$ and was approximately the same magnitude as N_V. These conditions imply that none of the terms in Equations 75, 76 or 77 could be neglected in a theoretical analysis. In this case the experimental Euler numbers were less than the theoretical Euler numbers.

Indications of the significance of the dimensionless parameters may still be observed even though their magnitudes did not differ enough to conclusively establish their importance. This may be done by noting the effects of changes of parameter values on the agreement between experimental and theoretical data.

Inspection of Figures 8 through 13 shows that the experimental data and the data plotted as curves labelled Pelech-Soo do not agree in general. The agreement does improve as either

the Reynolds number or the gap width or the radius ratio increases. The agreement becomes worse as the flow increases.

This variation in agreement follows with that expected from a consideration of appropriate variations in the dimensionless parameters listed in Table 9. As r_i, ω or s increase or as Q decreases, N_v becomes smaller, reflecting less influence of the terms related to the throughflow. Although N_v becomes smaller, increasing ω or s also increases $\frac{\omega s^2}{\nu}$ which implies an increasing significance of the convective terms related to the centrifugal fluid action and decreasing significance of the $\frac{v^2}{r}$ and $\frac{\partial^2}{\partial z^2}$ terms. Thus the theoretical equations, derived by assuming only the last two terms mentioned as being important, do not apply in this case.

CONCLUSIONS AND RECOMMENDATIONS

As indicated in the Introduction and Analysis sections, the prediction of the radial pressure distribution in a narrow gap between a rotating disk and a parallel stationary plate requires a knowledge of the velocity distributions present. This knowledge may be obtained by measuring the velocity distributions or by solving the equations governing the fluid flow. Since it is generally simpler to measure pressure distribution than velocity distributions, particularly in the narrow gaps involved in this investigation, the first attack on this problem was to measure the pressure distribution occurring on the stationary plate. The pressures were measured, referenced to atmospheric pressure and converted to Euler numbers as described in the Test Program section. The experimental data are presented in Figures 8 through 13 as points plotted on coordinates of Euler number versus radius ratio. The data presented were obtained from tests run under all combinations of Reynolds numbers of 1.80×10^5 and 3.01×10^5; N_F values of 41.35, 16.08 and 0.00; and six gap ratios between 0.006733 and 0.000958 (gap widths of 0.040 and 0.00575 inch).

Examination of the curves in Figures 8 through 13 reveals that Euler numbers increase as Reynolds number decreases, as flow increases or as gap width decreases. In general, the Euler numbers for zero flow appeared to be independent of Reynolds number in the ranges used. Inspection of Figures 8

and 9 shows that the variation of Reynolds number or N_F within the ranges in this investigation does not appreciably affect the values of Euler number for the two largest gap ratios used. The experimental results are discussed more fully in the Results section.

Examination of the governing equations revealed that in general they could not be solved as they are non-linear partial differential equations. A magnitude analysis performed on the governing equations after they had been non-dimensionalized indicated that the relative importance of certain groups of terms in the equations (75, 76 and 77) was related to the relative magnitudes of certain dimensionless parameters, which are tabulated in Table 9.

For narrow gaps, the terms associated with $\left(\frac{\omega r_o^2}{\nu}\right)^{-1}$ may be neglected since they are smaller by a factor equal to $\frac{s^2}{r_o^2}$ than the terms associated with $\left(\frac{\omega s^2}{\nu}\right)^{-1}$. The value of $\frac{s}{r_o}$ is approximately 10^{-3} for the narrow gap assumption. Thus the disk Reynolds number is not a significant parameter for flow problems of this type.

The only other linear terms from Equations 75, 76 and 77 are of a magnitude of 1, so the only time the governing equations reduce to a linear form is when the dimensionless parameters shown in Table 9 are much less than 1. This is the implicit assumption made by Pelech and Shapiro (13) and Soo (17) in their analyses. The closed form equation for the

pressure distribution (written in the form of Euler number) is either Equation 38 or 40.

Due's (6) work was apparently an attempt to obtain a pressure distribution equation without having to solve the non-linear governing equations which were applicable for his test work. Data calculated using his empirical equations 41 and 42 (developed using water as a fluid) agreed well with the experimental data from this investigation in the low flow and wide gap ranges (see Figures 8 through 13). His empirical analysis developed the same dimensionless parameters as were shown to be significant in this investigation except for $\frac{\omega s^2}{\nu}$.

The flow conditions present during the tests performed in this investigation were such that no terms from Equations 75, 76 or 77 could be neglected on the basis of the dominance of any dimensionless parameter. Thus the experimental data could not be used to conclusively verify the importance of the dimensionless parameters or their associated groupings of terms. Indications of the importance of the terms were obtained by noting the variation in agreement between the experimental and theoretical data as the magnitude of the associated dimensionless parameters changed. This is discussed in the Analysis section. The agreement varied as would be expected from an examination of the dimensionless parameters.

No numerical ranges could be associated with the influence of the dimensionless parameters because the experimental

work did not cover a wide enough range of variables to draw any conclusions.

The experimental data from this investigation are considered to be valid for the steady, incompressible, constant viscosity flow of a Newtonian fluid occurring in the range of variables listed in Tables 5, 6, 7, 10, and 11.

More test work is required to verify Equations 38 and 40 and to see if the variation in agreement between experimental and theoretical data is the same for high and low values of the dimensionless parameters listed in Table 9. It is also possible that the variation of agreement might not be the same for laminar flow as for turbulent flow. This would necessitate determination of the mode of flow, which could be done by using flow visualization techniques. The flow visualization techniques could also be used to determine the extent of inlet effects and the influence of inlet hole size on the flow characteristics of this problem.

The assumption of axially symmetric flow, made in the analysis, was not verified experimentally. Maroti, Deak and Kreith (11) found that the flow was not axially symmetric for very low throughflows in gaps ranging from 0.125 to 1.00 inch. An attempt was made to see if the flow variations noted in their work were present in this experimental work, but no meaningful results were obtained. Further work should be done using flow visualization techniques to verify this assumption

and further validate the analysis.

The work proposed is important not only because it concerns the applications of this flow situation which are discussed in the Introduction, but because it would fill a gap that exists in the present information available for this flow problem.

BIBLIOGRAPHY

1. Bayley, F. J. and Conaway, L. Fluid friction and leakage between a stationary and rotating disk. Journal of Mechanical Engineering Science 6: 164-172. 1964.

2. Beers, Yardley. Introduction to the theory of error. 2nd edition. Reading, Massachusetts, Addison-Wesley Publishing Co., Inc. 1957.

3. Daily, James W. and Arndt, Roger E. A. Enclosed rotating disks with superposed throughflow: a survey of basic effects. Massachusetts Institute of Technology Department of Civil Engineering Hydrodynamics Laboratory Report 53. 1962.

4. Daily, James W., Ernst, W. D. and Asbedian, V. V. Massachusetts Institute of Technology Department of Civil Engineering Hydrodynamics Laboratory Report 64. 1964.

5. Daily, James W. and Nece, R. E. Chamber dimension effects on induced flow and frictional resistance of enclosed rotating disks. American Society of Mechanical Engineers Transactions Series D, 82: 217-232. 1960.

6. Due, H. F., Jr. An empirical method for calculating radial pressure distribution on rotating disks. American Society of Mechanical Engineers Transactions Series A, 88: 188-196. 1966.

7. Hall, Newman A. Thermodynamics of fluid flow. Englewood Cliffs, New Jersey, Prentice-Hall, Inc. 1951.

8. Keenan, Joseph H. and Kaye, Joseph. Gas tables. New York, New York, John Wiley and Sons, Inc. 1948.

9. Kline, Stephen J. Similitude and approximation theory. New York, New York, McGraw Hill Book Company. 1965.

10. Kline, Stephen J. and McClintock, F. A. Describing uncertainties in single-sample experiments. Mechanical Engineering 75: 3-8. 1953.

11. Maroti, L. A., Deak, G. and Kreith, F. Flow phenomena of partially enclosed rotating disks. American Society of Mechanical Engineers Transactions Series D, 82: 539-552. 1960.

12. Pelech, Ivan. Flexible disk rotation next to a parallel plane. Microfilm copy. Unpublished Ph.D. thesis. Cambridge, Massachusetts, Library, Massachusetts Institute of Technology. 1962.

13. Pelech, Ivan and Shapiro, Ascher H. Flexible disk rotating on a gas film next to a wall. American Society of Mechanical Engineers Transactions Series E, 31: 577-584. 1964.

14. Peters, Leo Charles. Viscous shear torque generation between rotating plates. Unpublished M.S. thesis. Ames, Iowa, Library, Iowa State University of Science and Technology. 1963.

15. Popper, B. and Reiner, M. The application of the centripetal effect in air to the design of a pump. British Journal of Applied Physics 7: 452-453. 1956.

16. Reiner, M. A centripetal pump effect in air. International Congress for Applied Mechanics Actes 2: 429-438. 1956.

17. Soo, S. L. Laminar flow over an enclosed rotating disk. American Society of Mechanical Engineers Transactions 80: 287-296. 1958.

18. Taylor, Geoffrey and Saffman, P. G. Effects of compressibility at low Reynolds number. Journal of the Aeronautical Sciences 24: 553-562. 1957.

19. Welsh, William E., Jr. and Hartnett, James P. Velocity measurements in the boundary layer and in the main flow between two coaxial disks rotating with equal velocities in air. U.S. National Congress of Applied Mechanics Proceedings 3: 847-855. 1958.

ACKNOWLEDGMENTS

The author wishes to express his appreciation for the encouragement and guidance provided by Dr. George K. Serovy and Dr. Donald F. Young during this investigation.

Thanks are due Professor H. M. Black, Dr. Harry J. Weiss, Dr. Robert J. Lambert, Dr. Serovy and Dr. Young for their counsel during the course of the author's graduate study. The late Professor S. J. Chamberlin was also a valued source of advice and encouragement.

Financial support of this project by the President's Permanent Objective Committee, the I.S.U. Engineering Research Institute and the I.S.U. Department of Mechanical Engineering is gratefully acknowledged. The author is also very appreciative of the computer time, on the IBM 360 Model 50, that was provided by the I.S.U. Computation Center for the reduction of raw data and the calculation of comparative data.

The author is very grateful to Mr. Carmi Spicer, Mr. Ralph Long, Mr. Jim Clements, Mr. Clifford Osam, Mr. Alistair Robb and Mr. Aubrey Haight for their active assistance in developing and constructing the test fixture.

A special note of appreciation goes to the author's wife and children for their continued patience and encouragement throughout his entire graduate program.

APPENDIX: UNCERTAINTY ANALYSIS

This Appendix presents a discussion of the methods of measurement and the equipment used for obtaining experimental data in this investigation, as well as calculations of the uncertainty associated with the results determined from the data.

Kline and McClintock (10) define the uncertainty as an estimate, made by the investigator, of the possible size of the error associated with the determination of the value of a variable. The error in a given determination is the difference between the true value of the variable and the observed value of the variable. The actual error is seldom known because the true value of the variable is also seldom known.

The estimate of the uncertainty of any measurement is based on the experience of the investigator and any pieces of available information, such as calibration curves or observed fluctuations of the variable during the data taking.

The uncertainty of the results calculated from the data was determined using the following equation which may be found in either Kline and McClintock (10) or Beers (2). If R is the result and is a function of n independent variables v_1, v_2, $\cdots$, v_n, then the uncertainty of R, with the same odds as the uncertainty of each of the variables, is

$$\delta R = \left[\left(\frac{\partial R}{\partial v_1} \delta v \right)^2 + \left(\frac{\partial R}{\partial v_2} \delta v \right)^2 + \cdots + \left(\frac{\partial R}{\partial v_n} \delta v_n \right)^2 \right]^{\frac{1}{2}} . \qquad \text{(A-1)}$$

where

δR is the uncertainty of R in the same units as R

δv_i is the uncertainty of v_i in the same units as v_i, etc.

Stipulations accompanying Equation A-1 are that small errors are more likely than large errors, positive errors are as likely as negative errors and that all of the variables are independent.

The odds mentioned in conjunction with Equation A-1 are established by the investigator and represent the odds he would be willing to give in a wager that the true value of the variable being measured lies within the uncertainty limits specified.

If R is a function of the variables v_1, v_2 $\cdots$ v_n that has the following form

$$R = v_1^a \, v_2^b \cdots v_n^\alpha \ , \qquad \text{(A-2)}$$

then Equation A-1 may be divided on both sides by R with the following equation resulting

$$\text{Fractional Uncertainty} = \frac{\delta R}{R} = \left[\left(a\frac{\delta v_1}{v_1}\right)^2 + \left(b\frac{\delta v_2}{v_2}\right)^2 + \cdots + \left(\alpha\frac{\delta v_n}{v_n}\right)^2\right]^{\frac{1}{2}} . \quad \text{(A-3)}$$

The exponents a, b, $\cdots$, α may be positive or negative, integers, decimal numbers or fractions. The development of Equation A-3 for a specific case will be illustrated in one of the sets of calculations that follow.

The following paragraphs cover the determination of the uncertainty of each of the variables measured. All of the uncertainty intervals are established with 20 to 1 odds (i.e., the investigator is 95 percent certain that the true variable value lies within the specified uncertainty limits).

Temperature and Atmospheric Pressure

The temperature and atmospheric pressure were used to establish values of density and absolute viscosity for this investigation. Although the temperature and atmospheric pressure varied during the investigation as indicated below, the calculations following the temperature and atmospheric pressure discussion show that the density and the absolute viscosity may be considered as constants for these tests with an uncertainty of less than ±1.5 percent.

The variation of atmospheric pressure during the investigation was observed to be from 28.75 to 29.50 inches of

mercury. As this variation was much larger than the possible error in reading the barometer, the uncertainty was taken to be due only to the variation. Thus the atmospheric pressure, converted to pounds per square inch, for this investigation was 14.31 ± 0.18 psia.

Temperature measurements were made using copper-constantan thermocouples that were calibrated against a "certified" precision liquid-in-glass thermometer. Calibration results indicated that the recorded temperatures were within ± 1°F. All temperatures measured during the testing fell within the range 82 ± 4°F. The uncertainty of the temperature measurements was taken to include both the precision of the readings and the variation; thus the temperature for this test work was considered to be 82 ± 5°F.

Density

The density, used in the calculations of this investigation, was determined from the perfect gas law

$$\rho = \frac{p}{RT} \quad . \tag{A-4}$$

The mean density was found as

$$\rho_{mean} = \frac{p_{mean}}{RT_{mean}} = \frac{(14.31)(144)}{(53.3)(460 + 82)} = 0.0714 \frac{lb_m}{ft^3} \quad . \tag{A-5}$$

The uncertainty was determined using Equation A-3, which

was developed from Equation A-1 as follows. Equation A-1, written for the uncertainty of the density is

$$\delta\rho = \left[\left(\frac{\partial\rho}{\partial p}\delta p\right)^2 + \left(\frac{\partial\rho}{\partial T}\delta T\right)^2\right]^{\frac{1}{2}} . \qquad \text{(A-6)}$$

Now calculating the partial derivatives

$$\frac{\partial\rho}{\partial p} = \frac{1}{RT} \qquad \text{and} \qquad \frac{\partial\rho}{\partial T} = -\frac{p}{RT^2} .$$

If these partial derivatives are substituted into Equation A-6, and then both sides of the resulting equation are divided by ρ,

$$\frac{\delta\rho}{\rho} = \left[\left(\frac{\frac{1}{RT}\delta p}{\frac{p}{RT}}\right)^2 + \left(\frac{\left(-\frac{p}{RT}\right)(\delta T)}{\frac{p}{RT}}\right)^2\right]^{\frac{1}{2}} ,$$

$$\frac{\delta\rho}{\rho} = \left[\left(\frac{\delta p}{p}\right)^2 + \left(-\frac{\delta T}{T}\right)^2\right]^{\frac{1}{2}} . \qquad \text{(A-7)}$$

Then substituting numbers into Equation A-7,

$$\frac{\delta\rho}{\rho} = \left[\left(\frac{0.18}{14.31}\right)^2 + \left(\frac{5}{542}\right)^2\right]^{\frac{1}{2}} = 0.012 \text{ or } 1.2\% .$$

Thus the density, ρ, may be taken as $0.0714 \frac{lb_m}{ft^3} \pm 1.2$ percent for this investigation.

Viscosity

The absolute viscosity of the air was calculated using Sutherland's formula as found in Hall (7),

$$\mu = \frac{C_1 T^{\frac{3}{2}}}{T + C_2} , \qquad \text{(A-8)}$$

where C_1 is given as 2.22×10^{-8} and C_2 is given as 180 for air at pressures near atmospheric. Using this equation and the mean temperature as 542° Rankine, the mean value of the viscosity was found to be $3.86 \times 10^{-7} \frac{lb_f\text{-sec}}{ft^2}$, which checks closely with data found in Keenan and Kaye (8). The uncertainty was determined to be ± 0.7 percent from Equation A-1 modified to the form given as Equation A-3. Thus the absolute viscosity of the air in this investigation was taken to be $3.86 \times 10^{-7} \frac{lb_f\text{-sec}}{ft^2}$ ± 0.7 percent.

Pressure Difference

The pressure difference $p\text{-}p_o$, where p is the pressure in psf at any radius and p_o is the pressure in psf at the outer radius, will be abbreviated as Δp for ease of notation in the following discussion. Equation 31 in the Test Program section provides the pressure difference between any radius and the outer radius, and is repeated here

$$p\text{-}p_o = \Delta p = \left[\frac{p_{oi} - p_i}{F_i} + \frac{p_{ref} - p_{ref\text{-}o}}{F_{ref}}\right] 5.204 \qquad \text{(A-9)}$$

where 5.204 is the conversion factor for inches of water to pounds force per square foot.

The only uncertainty of the readings of p_{oi}, p_i, p_{ref} and p_{ref-o} was one-half the smallest scale reading (0.05 inch), since no fluctuations of manometer level were present during the investigation. The uncertainty of each of the calibration factors, δF_i, was determined from the calibration data and were all ± 0.2 or less for a nominal calibration factor of 10.0. The reference manometer tube had a calibration factor of 9.829 ± 0.170 inches of reading per inch of water. The values of the other calibration factors and their uncertainties will not be presented because they were good only for the manometer configuration of this investigation.

The equation for the uncertainty of Δp was obtained from Equation A-1 by substituting the appropriate partial derivatives of Equation A-9, the uncertainties of p_{oi}, p_i, p_{ref} and p_{ref-o}, the numerical values of F_{ref} and δF_{ref} and rearranging to get

$$\delta(\Delta p) = \left[0.005 \left(\frac{1}{F_i^2} + 0.01035 \right) + \left(\frac{(p_o - p_i)\,\delta F_i}{F_i^2} \right)^2 + \left(\frac{(p_{ref} - p_{ref-o})\,(0.170)}{(9.829)^2} \right)^2 \right]^{\frac{1}{2}} (5.204) \qquad \text{(A-10)}$$

This equation and Equation A-9 were programmed on the IBM 360/50 computer to calculate both Δp and the uncertainty of Δp. The percent uncertainty was also calculated for each pressure reading by dividing the uncertainty with the value of the pressure difference, then multiplying by 100.

Inspection of Equation A-10, while noting that $F_i \sim 10$ and $\delta F_i \sim 0.1$, reveals that the magnitude of the first term in the bracket is on the order of 10^{-4}, the second term is on the order of $10^{-6}(p_o-p_i)^2$ and the third term is on the order of $10^{-6}(p_{ref}-p_{ref-o})^2$. Since p_o-p_i was generally on the order of 1 and $(p_{ref}-p_{ref-o})$ was generally on the order of 0.1, the respective magnitudes were on the order of 10^{-4}, 10^{-6} and 10^{-8} for this investigation. Thus, for the majority of the pressure readings, the uncertainty was approximately constant and was a function mainly of the scale resolution. If the pressure drop was small, as most were, the percent uncertainty became large. Typical values for the uncertainty and percent uncertainty were, respectively, 0.05 pounds per square foot and 16 percent. A check of the calculated values of percent uncertainty disclosed that for approximately 95 percent of the data taken, the percent uncertainty of the pressure difference ranged between 12 and 20 percent.

Flow

The rate of air flow was measured using a Brooks Rotameter

Type 110. A monel ball float and a pyrex ball float were used for the range of air flows covered in this investigation. The air flow rate was set for a given run by increasing the air flow until the proper float was at the desired scale level. The five scale levels used were calibrated as discussed below.

Calibration was performed by measuring the volumetric rate of flow through the Rotameter using a Sargent wet test meter and a timer. The length of time required for one revolution of the pointer was recorded. Each revolution of the dial was 0.1008 ± 0.0007 ft^3 and the uncertainty of the timer was due to the resolution of the scale and was ± 0.05 seconds.

The Brooks Rotameter Co. presented the following equation for flow through the Rotameter

$$Q = Q_c \left(\frac{\rho_c}{\rho}\right)^{\frac{1}{2}} \qquad \text{(A-11)}$$

where Q and ρ are the values of the volumetric rate of flow and the density of the air at the desired state of operation and Q_c and ρ_c are the same quantities at calibration conditions. For the calibration, $Q_c = \frac{V}{\tau}$ where V is the volume of the Sargent wet test meter for one revolution and τ is the time in seconds for one revolution. Thus the equation for the flow for any setting of the Rotameter could be written as

$$Q = \frac{V}{\tau}\left(\frac{\rho_c}{\rho}\right)^{\frac{1}{2}} \quad . \qquad \text{(A-12)}$$

This equation is of the form for which Equation A-3 may be written, thus the propagation of uncertainty equation for a precise float setting may be written as

$$\frac{\delta Q}{Q} = \left[\left(\frac{\delta V}{V}\right)^2 + \left(-\frac{\delta \tau}{\tau}\right)^2 + \left(\frac{1}{2}\frac{\delta \rho_c}{\rho_c}\right)^2 + \left(-\frac{1}{2}\frac{\delta \rho}{\rho}\right)^2\right]^{\frac{1}{2}} . \qquad \text{(A-13)}$$

For $\delta V = 0.0007$ ft^3, $V = 0.1008$ ft^3, $\delta \tau = 0.05$ seconds, $\tau = 28.2$ seconds (the shortest time required for one revolution of the pointer during calibration) and $\frac{\delta \rho_c}{\rho_c} = \frac{\delta \rho}{\rho} = 0.012$, then $\frac{\delta Q}{Q} = 0.0088$.

In addition to the flow rate uncertainty resulting from the calibration data, uncertainty was also present due to fluctuation of the Rotameter float position for a given setting. These fluctuations were estimated to be $\pm \frac{1}{2}$ centimeter for the pyrex ball float and $\pm$ 2 centimeters for the monel ball float. Values of flow for the extremes of the fluctuations were obtained from the calibration curves and the total range of variation calculated. Half of this range was divided by the mean flow to obtain a fractional uncertainty due to the fluctuations, and this fractional uncertainty then added to the calibration uncertainty to obtain a value for the total uncertainty for each flow rate. These values are presented in Table 4 of the Test Program section.

Angular Velocity

The angular velocity was measured using a General Radio Co. Strobotac which had been calibrated against power line frequency as directed by the manufacturer. The manufacturer claimed an accuracy of ± 1 percent of dial reading after calibration. The angular velocity of the driving motor varied slightly during a run and, in addition, the rheostat controlling the motor speed was somewhat coarse in action. The resulting angular velocity was estimated to be within 10 rpm of the desired angular velocity. The resulting uncertainty on any angular velocity setting was considered to be ± 1 percent ± 10 rpm. The uncertainty associated with each angular velocity is given in Table 4 of the Test Program section.

Gap Width

The procedure for determining the average gap width is described in the Test Program section. The average value of the gap width is obtained by averaging eight measurements of gap width (four measurements are taken at holes 4, 5, 6 and 9, then the disk is rotated approximately 90° for another set of four measurements at the same holes). Thus,

$$S_{avg} = \frac{S_1 + S_2 + S_3 + S_4 + S_5 + S_6 + S_7 + S_8}{8} . \qquad \text{(A-14)}$$

The uncertainty of each reading is one-half the smallest

division on the depth micrometer used, 0.0005 inch, and is the same for all readings. Thus Equation A-1 applied in this case provides the following value for the gap width uncertainty

$$\delta s = \left[\frac{8(0.0005)^2}{64}\right]^{\frac{1}{2}} = 0.00018 \text{ inch} \quad .$$

The maximum percent uncertainty occurs on the narrowest gap, and thus would be $\left(\frac{0.00018}{0.005}\right) \times 100 = 3.6$ percent.

Euler Number

The percent uncertainty of the experimentally determined Euler number is very close to the percent uncertainty of the pressure drop. This may be shown by writing Equation A-3 for the Euler number. The Euler number is defined in this investigation as

$$\text{Euler number} = \frac{p-p_o}{\frac{1}{2}\rho\omega^2 r_o^2}(\text{dimensionless}) \quad . \qquad \text{(A-15)}$$

Equation A-3 for the Euler number is written as

$$\frac{\delta(\text{Euler number})}{\text{Euler number}} = \left[\left(\frac{\delta(p-p_o)}{(p-p_o)}\right)^2 + \left(-\frac{\delta\rho}{\rho}\right)^2 + \left(-2\frac{\delta\omega}{\omega}\right)^2 + \left(-2\frac{\delta r_o}{r_o}\right)^2\right]^{\frac{1}{2}} .$$

(A-16)

Values for the variables in the above equations have been previously presented in this Appendix except for δr_o which is

one-half the smallest division of the micrometer scale, 0.0005 inch, and r_o which is 6 inches. If the values for the average percent uncertainty of $(p-p_o)$, percent uncertainty of ρ, worst percent uncertainty of ω and the values for δr_o and r_o are substituted into Equation A-16, the following expression results

$$\frac{\delta(\text{Euler number})}{\text{Euler number}}$$

$$= \left[(0.16)^2 + (-0.012)^2 + (-[2][0.0183])^2 + (-[2][\frac{0.0005}{6}])^2\right]$$

$$= \left[0.0256 + 0.000144 + 0.00133 + 0.00000003\right]^{\frac{1}{2}}$$

The dominating term results from the uncertainty of the pressure difference and is at least one order of magnitude greater than any of the terms resulting from the other uncertainties. Therefore, the percent uncertainty of the Euler number is very close to that of the pressure difference. This is confirmed by the computer calculations, so the percent uncertainty of any Euler number presented in this investigation ranges from 12 to 20 percent for 95 percent of the calculated Euler numbers.